



Intercomparison of daytime stratospheric NO₂ satellite retrievals and model simulations

M. Belmonte Rivas¹, P. Veefkind^{1,2}, F. Boersma², P. Levelt^{1,2}, H. Eskes², and J. Gille³

¹Technical University of Delft, Delft, the Netherlands

²Royal Netherlands Meteorology Institute, De Bilt, the Netherlands

³National Center for Atmospheric Research, Boulder CO, USA

Correspondence to: M. Belmonte Rivas (m.belmonterivas@tudelft.nl)

Received: 20 December 2013 – Published in Atmos. Meas. Tech. Discuss.: 30 January 2014

Revised: 7 May 2014 – Accepted: 12 June 2014 – Published: 22 July 2014

Abstract. This paper evaluates the agreement between stratospheric NO₂ retrievals from infrared limb sounders (Michelson Interferometer for Passive Atmospheric Sounding (MIPAS) and High Resolution Dynamics Limb Sounder (HIRDLS)) and solar UV/VIS backscatter sensors (Ozone Monitoring Instrument (OMI), Scanning Imaging Absorption Spectrometer for Atmospheric Cartography (SCIAMACHY) limb and nadir) over the 2005–2007 period and across the seasons. The observational agreement is contrasted with the representation of NO₂ profiles in 3-D chemical transport models such as the Whole Atmosphere Community Climate Model (WACCM) and TM4. A conclusion central to this work is that the definition of a reference for stratospheric NO₂ columns formed by consistent agreement among SCIAMACHY, MIPAS and HIRDLS limb records (all of which agree to within 0.25×10^{15} molecules cm⁻² or better than 10 %) allows us to draw attention to relative errors in other data sets, e.g., (1) WACCM overestimates NO₂ densities in the extratropical lower stratosphere, particularly in the springtime and over northern latitudes by up to 35 % relative to limb observations, and (2) there are remarkable discrepancies between stratospheric NO₂ column estimates from limb and nadir techniques, with a characteristic seasonally and latitudinally dependent pattern. We find that SCIAMACHY nadir and OMI stratospheric columns show overall biases of -0.5×10^{15} molecules cm⁻² (−20 %) and $+0.6 \times 10^{15}$ molecules cm⁻² (+20 %) relative to limb observations, respectively. It is argued that additive biases in nadir stratospheric columns are not expected to affect tropospheric retrievals significantly, and that they can be attributed to errors in the total slant column density, related either to

algorithmic or instrumental effects. In order to obtain accurate and long-term time series of stratospheric NO₂, an effort towards the harmonization of currently used differential optical absorption spectroscopy (DOAS) approaches to nadir retrievals becomes essential, as well as their agreement to limb and ground-based observations, particularly now that limb techniques are giving way to nadir observations as the next generation of climate and air quality monitoring instruments pushes forth.

1 Introduction

Nitrogen dioxide (NO₂) is a major air pollutant in the troposphere produced mainly from fossil fuel burning, but also from biomass burning, microbial soil activity and lightning (Lamarque, 1996). In the stratosphere, NO₂ is a major ozone-depleting substance produced primarily from the oxidation of nitrous oxide (N₂O), which in turn arises from biogenic sources in soils, oceans and cultivated areas. In contrast, stratospheric NO₂ acts as a protection against halogen-driven ozone loss by converting reactive chlorine, bromine and hydrogen compounds into stable reservoir species such as ClONO₂, BrONO₂ and HNO₃ (Wennberg et al., 1994). Denitrification, or the removal of stratospheric NO₂ through formation and deposition of polar stratospheric ice particles, is a key microphysical process in the formation of polar ozone holes (Farman et al., 1985). However, the representation of denitrification remains unrealistic in current chemical transport models (CTMs) during cold winters (WMO, 2003). Also for long-term trend studies, stratospheric NO₂ remains

subject to changes in Br and Cl loadings, and a trend in N₂O emissions of 2.5 % decade⁻¹ that could lead to further changes in stratospheric ozone concentrations (Ravishankara et al., 2009). The maintenance of a reliable and accurate system for the monitoring of stratospheric NO₂ is thus justified.

The monitoring of stratospheric NO_x, which began with the early work of Noxon (1979), continued into the satellite era with the first vertically resolved profiles from LIMS (Limb Infrared Monitor of the Stratosphere) and the longer continuous data sets from solar occultation instruments like Stratospheric Aerosol and Gas Experiment (SAGE), Halogen Occultation Experiment (HALOE), Polar Ozone and Aerosol Measurement (POAM) and Atmospheric Chemistry Experiment–Fourier Transform Spectrometer (ACE-FTS). Various limb emission and scattering instruments have also followed, like OSIRIS, High Resolution Dynamics Limb Sounder (HIRDLS), Michelson Interferometer for Passive Atmospheric Sounding (MIPAS) and Scanning Imaging Absorption Spectrometer for Atmospheric Cartography (SCIAMACHY), along with the nadir UV/VIS backscattering observations from GOME, SCIAMACHY and Ozone Monitoring Instrument (OMI), and the lunar occultations from GOMOS. The role of the NDACC of ground-based stations (Network for the Detection of Atmospheric Composition Change) as a monitoring reference for stratospheric NO₂ also deserves to be mentioned, just as dedicated modeling evaluation efforts such as Stratospheric Processes And their Role in Climate (SPARC) Chemistry Climate Model Validation (CCMVal) (Eyring et al., 2010) to obtain a better understanding of stratospheric chemistry and its relation to the long-term evolution of the ozone layer.

While recent work has acknowledged the need to investigate differences in satellite stratospheric NO₂ columns (Krotkov et al., 2012) and profiles (Hegglin and Tegtmeier, 2014), this work sets out to actually characterize the extent to which observation systems are consistent with one another. This paper is structured as follows. Section 2 provides a description of the raw satellite and model-based data sets that intervene in the intercomparison: the satellite records in Sect. 2.1, the model-based photochemical correction in Sect. 2.2 and the model simulations in Sect. 2.3. Section 3 contains our main results, with the gradual inclusion of limb profiles (Sect. 3.1), model profiles (Sect. 3.2) and nadir vertical columns (Sect. 3.3) into the comparison, followed by some discussion. Finally, Sect. 4 brings a summary and our conclusions.

2 Methodology

2.1 Satellite observations

Global and daily maps of tropospheric and stratospheric NO₂ amounts are provided routinely by satellite remote sensors. Limb sounders like HIRDLS, MIPAS and SCIAMACHY

(in limb mode) collect infrared thermal or UV/VIS solar backscattered radiation arising from the Earth's horizon to provide records of vertical trace gas profiles across the stratosphere. Limb sounders, however, have difficulty observing the tropospheric NO₂ component due to the extremely long optical paths that arise in the limb geometry. The optical path through the troposphere is minimized in nadir geometry, so UV/VIS nadir sounders like OMI, SCIAMACHY (in nadir mode) and GOME are the only satellite sensors currently capable of providing information on the tropospheric NO₂ component. The difficulty with nadir measurements, however, lies in their low vertical resolution, which is related to the inability to separate the stratospheric and tropospheric contributions, particularly when more than 90 % of the observed NO₂ column resides in the stratosphere, as over unpolluted regions (Dirksen et al., 2011).

2.1.1 Limb sounders

SCIAMACHY limb

The UV/VIS spectrometer SCIAMACHY (Scanning Imaging Absorption Spectrometer for Atmospheric Cartography; Bovensmann et al., 1999) was launched aboard the ESA satellite ENVISAT (Environment Satellite) in a Sun-synchronous orbit with a 10:00 local solar time (LST) at the descending node. The limb retrieval of NO₂ from SCIAMACHY (SCIA-Arc data version 3.1, <http://www.iup.uni-bremen.de/scia-arc>) is performed by IUP Bremen in the 420–470 nm wavelength range with a vertical resolution of 3–4 km using ratios of radiance spectra referenced to a common tangent height around 40 km. The retrieval takes into account the absorption by NO₂ (Bogumil et al., 2003), ozone and O₂–O₂, the Ring effect, undersampling and stray light corrections, and a third-order polynomial – which accounts for smooth spectral features arising from surface albedo, and Rayleigh and Mie scattering/absorption contributions. A constant surface albedo and a background stratospheric aerosol scenario are included in the forward model. The explicit temperature dependence of the cross sections is considered via European Center for Medium Range Weather Forecast (ECMWF) profiles (Rozanov, 2008).

MIPAS

The limb sounder MIPAS (Michelson Interferometer for Passive Atmospheric Sounding; Fischer et al., 2008) is a Fourier transform infrared spectrometer flying aboard the ESA satellite ENVISAT in a Sun-synchronous orbit with a 10:00 LST at the descending node. Infrared limb sounders like MIPAS and HIRDLS measure the thermal emission that arises from the atmosphere to yield the concentration of a specific absorber/emitter along the limb path. This type of retrieval requires knowledge of the layer temperature and pressure, which is solved preliminarily using channels that target gases

with known mixing ratio, like CO₂. The NO₂ volume mixing ratio (VMR) profile is retrieved using three narrow-band channels (about 3 cm⁻¹) centered about the NO₂ ν_3 band (6.2 μ m) with a vertical resolution of 3–5 km. The retrieval takes into account interfering contributions from H₂O and CH₄ (IMK-IAA version 4.0; von Clarmann et al., 2003; Funke et al., 2005) and MIPAS temperature and pressure profiles retrieved from multiple narrow channels located on the high-frequency side of the main 15 μ m CO₂ band.

HIRDLS

The limb sounder HIRDLS (High Resolution Dynamics Limb Sounder; Gille et al., 2003) is an infrared radiometer flying aboard the NASA Earth Observing System (EOS) satellite Aura in a Sun-synchronous orbit with a 13:45 LST at the ascending node. The NO₂ VMR profile is retrieved using a single wide-band channel (about 30 cm⁻¹) centered about the NO₂ ν_3 band (6.2 μ m) with a vertical resolution of 1 km, and taking into account contributions from H₂O, CH₄ and the O₂ pressure-induced continuum (Lambert et al., 1999). As with MIPAS, temperature and pressure profiles are retrieved using multiple channels located on the low-frequency side of the main 15 μ m CO₂ band. A radiometric correction algorithm has been applied as detailed by Gille et al. (2008) to account for the radiative contamination (background biases and drifts) arising from a piece of thermal insulation that became detached during launch and partially blocked the instrument aperture. Because of the partial blockage, the daytime HIRDLS measurements are collected at 15:00 LST over the Equator (Eq). The present HIRDLS data release is version 7 (Gille et al., 2012a, b).

2.1.2 Nadir sounders

UV/VIS nadir sounders like OMI and SCIAMACHY measure the solar radiation reflected back from the Earth's surface and atmosphere. The measured reflectance spectra (i.e. the ratio of top-of-atmosphere radiance to direct solar irradiance) yield the concentration of absorbing gas integrated along the effective light path through the atmosphere. The slant column density is then converted to a vertical column density using an air mass factor (AMF) derived from a radiative transfer calculation, which is based on a number of assumptions regarding the distribution of absorbers and scatterers (Burrows et al., 2011). The separation between stratospheric and tropospheric components is carried out with the help of a CTM, as detailed below. The OMI and SCIAMACHY nadir products (as derived from KNMI and KNMI-BIRA slant column retrievals, respectively) are available at www.temis.nl/airpollution/no2.html.

OMI

The UV/VIS spectrometer OMI (Ozone Monitoring Instrument; Levelt et al., 2006) was launched aboard the NASA EOS Aura, alongside with HIRDLS, in a Sun-synchronous orbit with a 13:45 LST at the ascending node. The nadir retrieval (KNMI DOMINO version 2.0) estimates total slant columns of NO₂ based on specific narrow-band absorption features in the Earth reflectance spectrum. The retrieval minimizes differences between model and observed reflectance spectra over the 405–465 nm spectral window using a spectral resolution of 0.63 nm, and taking into account the absorption by NO₂, ozone, water vapor, the Ring effect and a fifth-order polynomial – which accounts for smooth spectral features arising from surface albedo, and Rayleigh and Mie scattering/absorption contributions (Boersma et al., 2007, 2011). The NO₂ cross-section spectrum for 220 K is taken from Vandaele et al. (1998) and convolved with the OMI instrument transfer function (Dirksen et al., 2006). This retrieval uses a solar irradiance climatology established for the year 2005 as the reference spectrum. A correction for the temperature sensitivity of the NO₂ spectrum is introduced in the air mass factor calculation using an effective column temperature derived from ECMWF temperature and CTM gas profiles (Boersma et al., 2004).

SCIAMACHY nadir

The nadir retrieval (KNMI-BIRA TM4NO2A version 2.3) is effected over the 426–451 nm spectral window using a spectral resolution of 0.44 nm. It takes into account the absorption by NO₂, ozone, water vapor and O₂–O₂, an undersampling cross section, the Ring effect (Vountas et al., 1998) and a second-order polynomial. The NO₂ cross section for 243 K is taken from Bogumil et al. (1999). A correction for the temperature sensitivity of the NO₂ spectrum is introduced in the AMF calculation using the same scheme applied to OMI retrievals (Boersma et al., 2004). Because of a lack of usable solar spectra, the KNMI-BIRA retrievals use an Earth radiance spectrum over the Indian Ocean as the reference spectrum, which is corrected for the signature of an assumed 1.5×10^{15} molecules cm⁻² vertical stratospheric NO₂ column (ensuring long-term consistency with KNMI-BIRA retrievals from GOME; van der A et al., 2006).

Stratospheric and tropospheric columns

The total slant column N_s retrieved from the nadir instrument (using a cross section for NO₂ absorption at a fixed temperature) is transformed into a total vertical column N_v via the air mass factor M as

$$N_v = N_s / M, \quad (1)$$

with

$$M = \sum_z m(z) \cdot c[T(z)] \cdot n_{v0}(z) / N_{v0}, \quad (2)$$

where $m(z)$ is the scattering weighting function (Palmer et al. (2001) also vertically resolved air mass factor or sensitivity, usually derived from a radiative transfer calculation as a function of surface albedo and pressure, cloud fraction and pressure, and viewing geometry – independent of absorber distribution for an optically thin gas); n_{v0} is an a priori vertical trace gas profile extracted from a CTM – with total sum N_{v0} across the layer; and $c[T(z)]$ is a correction for the temperature sensitivity of the NO₂ cross section (Boersma et al., 2004). The temperature correction is expressed as

$$c(T) = \frac{N_s(T_{\text{ref}})}{N_s(T)} = (T_{\text{ref}} - 11.4) / (T - 11.4) \quad (3)$$

as a function of the reference temperature chosen for the spectral fit retrieval, namely $T_{\text{ref}} = 243$ K for SCIAMACHY nadir and $T_{\text{ref}} = 220$ K for OMI. The air mass factor M can be interpreted as the column-weighted sensitivity of the slant measurement. The separation between stratospheric and tropospheric components is carried out via assimilation of measured slant columns into a chemical transport model (i.e., TM4 described in Sect. 2.3.2). The assimilation of stratospheric NO₂ columns from the OMI and SCIAMACHY nadir total columns proceeds as

$$y = H \cdot x, \quad (4)$$

where $y = N_s / M_{\text{geo}}$ is the measured slant column N_s normalized by the geometric air mass factor M_{geo} defined below, $x = n_v(z)$ is the assimilated trace gas profile and

$$H(z) = M \cdot A(z) / M_{\text{geo}} \quad (5)$$

is the observation operator with averaging kernel $A(z)$ and normalized by the geometric air mass factor M_{geo} , defined as a function of the solar zenith angle (SZA) and satellite viewing line of sight (LOS) angle as

$$M_{\text{geo}} = 1 / \cos(\text{LOS}) + 1 / \cos(\text{SZA}). \quad (6)$$

The averaging kernel $A(z)$ is constructed as in Eskes and Boersma (2003) as

$$A(z) = m(z) \cdot c[T(z)] / M. \quad (7)$$

And the assimilation update proceeds in a Kalman filter fashion as

$$x - x_0 = \text{VH}^T (\text{HVH}^T + S)^{-1} (y - Hx_0), \quad (8)$$

where x_0 is the a priori trace gas profile $n_{v0}(z)$ provided by the CTM. This equation implies that, as long as the observation noise covariance S is small, changes in the assimilated

gas profile $(x - x_0)$ are driven by changes in the observed slant column $(y - Hx_0)$. The observation noise covariance is defined as

$$S = (4 \cdot N_{\text{S0,trop}} + 0.25 \cdot N_{\text{S0,strat}}) / N_{\text{S0}}, \quad (9)$$

which guarantees that the observation error becomes unacceptable as soon as the a priori model tropospheric component is larger than about 0.5×10^{15} molecules cm⁻² (Boersma et al. (2007) note that typical values for the tropospheric and stratospheric slant columns, $N_{\text{s,trop}}$ and $N_{\text{s,strat}}$, over clean backgrounds are 0.2 and $2 \times M_{\text{geo}} \times 10^{15}$ molecules cm⁻², respectively). Thus only measurements with expected low tropospheric components are used to update the model gas profiles. The a priori state covariance V is formulated such that $V \cdot (1 \dots 1)^T$ is proportional to the model gas profile $n_{v0}(z)$ (simultaneously enforcing a horizontal correlation length of 600 km; Dirksen et al., 2011). This implies that the vertical dependence of the increments made to model gas profiles is proportional to VH^T according to Eq. (8), i.e., proportional to the model gas profile times the averaging kernel, so that

$$n_v(z) = n_{v0}(z) \cdot (1 + \alpha \cdot A(z)), \quad (10)$$

where α is a scalar driven by the difference between observed and model vertical columns over clean areas. This constraint forces profile adjustments made in assimilation to ignore levels where the kernel is small, mostly in the troposphere, and take place in the stratosphere, where the kernel approaches unity, so that the shape of the model gas profile is also preserved. In summary, the assimilation adjusts the model profiles to match slant column observations over unpolluted areas, while preserving the shape of the stratospheric profile and leaving the expected clean tropospheric background largely unchanged. The assimilated information is then advected over polluted areas via atmospheric transport. The assimilation root mean square error (i.e., the standard deviation of the differences between observed and assimilated NO₂ columns over clean areas) is 0.25×10^{15} molecules cm⁻².

2.2 Photochemical correction

Diurnal NO₂ variation

NO₂ belongs to the odd nitrogen group (NO_y), which is a long-lived family with a lifetime of about 1 year formed primarily in the tropical mid-stratosphere via oxidation of N₂O, and mainly composed of NO, NO₂, N₂O₅, HNO₃ and ClONO₂. NO₂ is a short-lived gas in fast photochemical equilibrium with NO, whose sum is referred to as NO_x. At night, all NO_x is in the form of NO₂. But over daytime, a photochemical balance between NO₂ and NO is maintained by two rapid processes: the photolysis of NO₂ into NO and the oxidation of NO into NO₂ via ozone, in a cycling that takes place on a timescale of about 1 min – and which is strongly

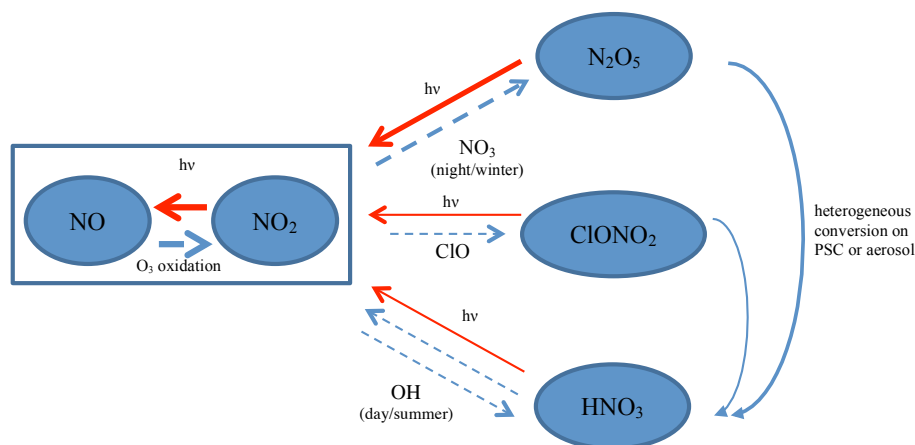


Figure 1. Schematic depiction of relevant interactions between nitrogen species in the stratosphere.

dependent on temperature and ozone concentration (Brasseur et al., 1999). After a rapid NO/NO₂ balance, the evolution of total stratospheric NO_x is controlled by sunlight-driven exchange with the other main reservoir nitrogen species: HNO₃ (lifetime of weeks), N₂O₅ (lifetime of hours to days) and CIONO₂ (lifetime of hours).

As schematically pictured in Fig. 1, NO_x production occurs primarily by photodissociation of N₂O₅ during daytime. Other but much slower daytime production paths are HNO₃ photolysis, CIONO₂ photolysis (i.e., chlorine activation) and reaction of HNO₃ with OH, all of them occurring primarily below 35 km. Removal of NO_x occurs mainly through formation of N₂O₅ at nighttime, which also reacts in a way similar to CIONO₂ on liquid/solid surfaces (such as background aerosols or polar stratospheric clouds) to form HNO₃. Other minor NO_x removal paths are the daytime formation of HNO₃ through reaction with the OH radical and the formation of CIONO₂, i.e., chlorine deactivation (Brasseur and Salomon, 2005). In contrast to N₂O₅, which is exclusively formed at night, HNO₃ is formed continuously: the nighttime gas phase production of HNO₃ and CIONO₂ may drop to zero, as OH disappears and CIO gradually goes away, but heterogeneous formation of HNO₃ continues mainly at the expense of N₂O₅.

In summary, the diurnal evolution of NO₂ results from the sunlight-driven balance between NO and NO₂, externally bound to a total NO_x amount, which is almost entirely explained by nighttime formation and daytime breakup of N₂O₅. In the lower stratosphere, additional reactions involving formation of HNO₃ and CIONO₂ also affect the total NO_x available. As shown in Fig. 2, the stratospheric NO₂ VMR features a broad maximum between 30 and 40 km (10–3 hPa) with a large drop at sunrise, as photodissociation brings NO₂ back in balance with NO. The daytime (night-time) concentrations increase (decrease) gradually, reflecting the slow increase (decrease) in total NO_x that mainly results from the breakup (formation) of N₂O₅.

Photochemical correction

The strong diurnal NO₂ cycle complicates the comparison of satellite measurements taken at different local solar times (Hegglin and Tegtmeier, 2014). Figure 3 illustrates the sampling attributes of the limb and nadir instruments included in this study over a single orbital pass. The HIRDLS instrument covers the latitude range of 64° S to 80° N with an ascending node at 15:30 LST, a longitudinal spacing of 25° (3000 km) at the Equator and 100 km spacing along track. Both MIPAS and SCIAMACHY cover the entire 90° S to 90° N latitude range, with an along-track spacing of 500 and 800 km for MIPAS and SCIAMACHY, respectively; a descending node at 10:00 LST; and a longitudinal spacing of 25° degrees. As an imager, OMI shows a denser sampling capacity with along- and across-track spacing of 13 and 24 km, respectively; a 2600 km swath width; and an ascending node at 13:45 LST.

A photochemical model is introduced to correct for differences in local solar time between the different instruments. The photochemical correction (alias photocorrection) is effected via the ratio of model zonal mean NO₂ profiles evaluated at a given latitude (lat) and appropriate observation times (LST, LST₀) as

$$\text{VMR}(z, \text{lat}, \text{doy}, \text{LST}) = \text{VMR}(z, \text{lat}, \text{doy}, \text{LST}_0) \cdot \frac{\text{VMR}_{\text{model}}(z, \text{lat}, \text{doy}, \text{LST})}{\text{VMR}_{\text{model}}(z, \text{lat}, \text{doy}, \text{LST}_0)}, \quad (11)$$

where z refers to altitude and doy to day of year. The photochemical correction is based on the Whole Atmosphere Community Climate Model (WACCM) described in Sect. 2.3.1. All the satellite records have been diurnal cycle corrected to HIRDLS LST (see Fig. 3) using altitude-, latitude- and season-dependent scaling factors. Figure 4 shows representative column-averaged photocorrection factors, which roughly amount to 5–10 % increases for OMI columns and 10–30 % increases for MIPAS and SCIAMACHY columns. The large

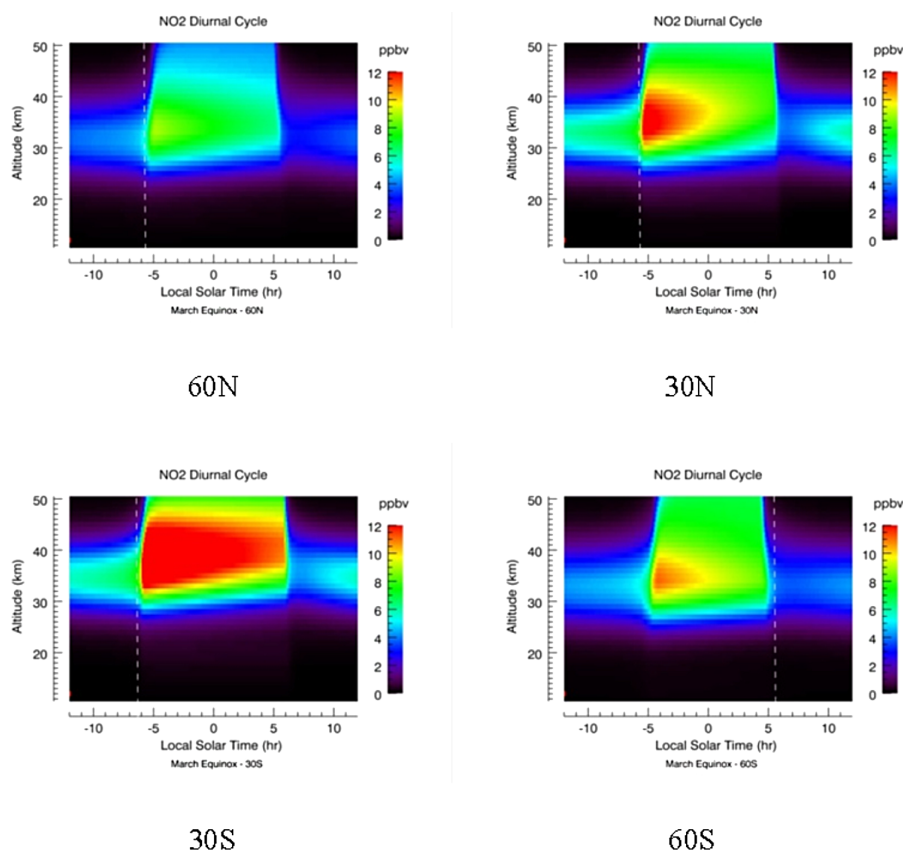


Figure 2. Diurnal variation of NO₂ (21 March 2005) from the photochemical model described in McLinden et al. (2000).

wintertime photocorrection factors in Fig. 4, south of 50° S in the austral winter or north of 60° N in the boreal winter, correspond to latitude sectors that suffer daytime-to-nighttime conversions at large solar zenith angles, and should be treated with caution. Errors introduced by the photocorrection, which assumes that the aspects controlling the diurnal NO₂ cycle (such as stratospheric temperature and the rate of photolytic decay of N₂O₅) have much stronger latitudinal than longitudinal dependencies, and may include uncertainties regarding kinetic reaction rates and photolysis cross sections, are expected to be less than 10 % in the middle stratosphere and 20 % in the lower/upper stratosphere over extrapolar latitudes. Larger uncertainties are expected over regions where transport dynamics dominate over chemistry, such as the edge of the winter polar vortex (north of 45° in the winter hemisphere) and close to the upper troposphere–lower stratosphere (UTLS, below approximately 50 hPa).

2.3 Model simulations

SD-WACCM

The SD-WACCM (Whole Atmosphere Community Climate Model with specified dynamics, version 4) is used in this work to perform the diurnal cycle corrections detailed in

Sect. 2.2. It is a full global climate model with chemistry based on the Community Atmospheric Model (CAM) featuring 66 vertical levels from the ground to approximately 145 km, and all the physical parameterizations described by Richter et al. (2008). The dynamical fields of temperature and wind are specified by MERRA reanalyses (Rienecker et al., 2011). The gravity wave drag and vertical diffusion parameterizations are described in Garcia et al. (2007). WACCM has a detailed neutral chemistry module for the middle atmosphere, including ClO_x and BrO_x reactions and diurnal cycles for all constituents at all levels in the model domain. The stratospheric aerosol is initialized with the SAGE II climatology, with additional information on heterogeneous processes included in Kinnison et al. (2007). Vertical resolution is ≤ 1.5 km between the surface and about 25 km, increasing to 2 km at the stratopause and 3.5 km in the mesosphere. The latitude and longitude grids have spacing of 1.9 and 2.5°, respectively, and the time step is 30 min. A slightly older version of this WACCM (version 3.5.48) was included, along with 17 other chemistry climate models (CCMs), in the SPARC CCMVal2 study (Eyring et al., 2010) assessing the confidence that can be placed on CCMs to represent key processes for stratospheric ozone and its impact in climate. As far as stratospheric dynamics, transport

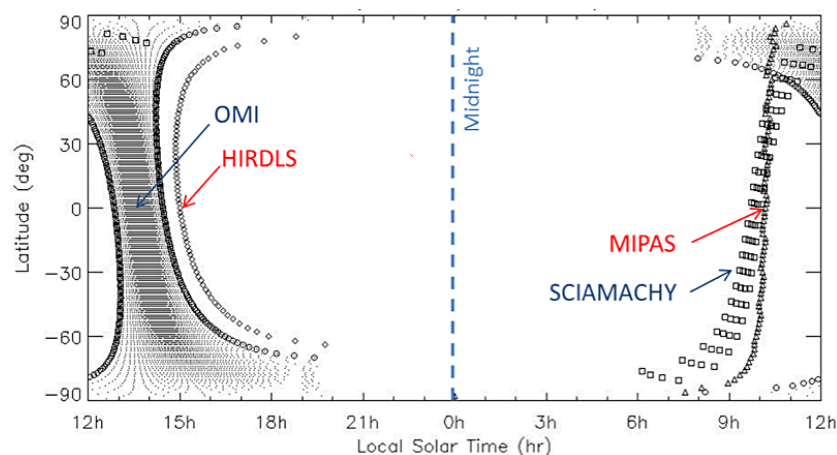


Figure 3. Daytime local solar times (LST) for different satellite observations: OMI and HIRDLS fly on the same EOS Aura platform, yet their viewing geometries result in different local solar times. The same occurs to MIPAS and SCIAMACHY on ESA's ENVISAT.

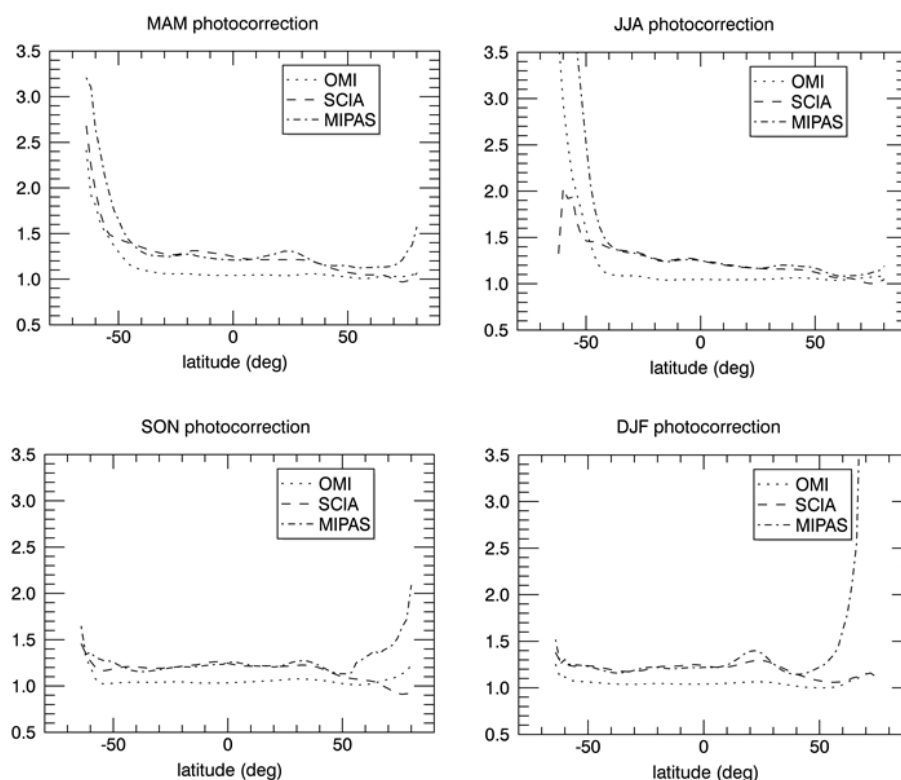


Figure 4. Seasonal average (MAM, JJA, SON and DJF) of OMI, MIPAS and SCIAMACHY column photocorrection (diurnal cycle correction) factors plotted as a function of latitude.

and chemistry were concerned, WACCM performed overall better than average in that validation study.

TM4

The TM4 chemistry transport model is used for the assimilation (i.e., separation of the stratospheric and tropospheric components) of the OMI and SCIAMACHY slant columns.

Only assimilated profiles are analyzed here. The latitude and longitude grids have spacings of 2 and 3°, respectively, with 35 sigma pressure levels up to 0.38 hPa. The horizontal and vertical transport of species is based on dynamical fields of temperature and wind specified by the ECMWF reanalyses. The physical parameterizations for convective tracer transport, boundary layer diffusion and mass conserved tracer

Table 1. Number of daily zonal mean SCIAMACHY–MIPAS–HIRDLS collocations in the 2005–2007 period.

No. collocations	SCIA-MIP	SCIA-HIR	HIR-MIP	Three-way
MAM	79	142	58	55 days out of 276
JJA	104	191	97	88 days out of 276
SON	99	237	108	93 days out of 276
DJF	89	174	91	70 days out of 276

advection are as in Tiedtke (1989), Louis (1979) and Russell and Lerner (1981). The tropospheric chemical scheme is based on Houweling et al. (1998) using the POET emissions database (Olivier et al., 2003). The stratospheric chemistry scheme accounts for O_x–NO_x–HO_x reactions including the conversion of NO and NO₂ to N₂O₅ and HNO₃, but other aspects such as the photolysis of N₂O and reactions with halogens are missing. To compensate for the simplified chemistry in the stratosphere, ozone concentrations are nudged to climatology above 50 hPa. Above 10 hPa, stratospheric HNO₃ is nudged to the UARS-derived O₃/HNO₃ ratio, and stratospheric NO_x is nudged to its value at 10 hPa (Dirksen et al., 2011).

3 Results and discussion

3.1 Limb measurements

The intercomparison between satellite stratospheric NO₂ data sets starts with daily zonally averaged partial column profiles collected from limb sounders over the 2005–2007 period and covering the pressure range from 0.1 to 300 hPa using 2° latitude bins. The number of three-way coincidences between SCIAMACHY limb, MIPAS and HIRDLS, which is mainly limited by missing data in the MIPAS record over 2005–2006 (due to an instrumental anomaly) and some HIRDLS flagged data (Gille et al., 2012a), is listed in Table 1. The seasonal averages created from the three-way collocated data sets are shown in Figs. 5–6 and remain representative of climatology to 5–10 % in light of the WACCM intraseasonal variability. Recall that all data sets have been photocorrected to HIRDLS local solar times.

The partial column profiles $n_v(z)$ are calculated as

$$n_v(z_i) = 10 \cdot N_A / (g \cdot M_{\text{air}}) \cdot 0.5 \cdot (\text{VMR}_{i+1} + \text{VMR}_i) \cdot (p_{i+1} - p_i), \quad (12)$$

where N_A is Avogadro's constant (6.022×10^{23} molecules mol^{−1}), g is the Earth's gravity (9.80 m s^{−2}), M_{air} is the molar mass of air (28.97 g mol^{−1}) and VMR is the gas volume mixing ratio. Partial column profiles are calculated on a standard grid with uniformly spaced log-pressure levels defined as $p(i) = 1000.0 \times 10^{-i/24}$ for $i = 0, 120$ in hPa over the MAM, JJA, SON and DJF seasons and over Southern Hemisphere (SH, 30° S–60° S), tropical

(30° N–30° S) and Northern Hemisphere (NH, 30° N–60° N) latitude sectors. Excluded from the statistics are polar latitudes north of 60° N and south of 60° S. The comparison scores, including mean relative difference (MRD) and standard deviation (SD), are summarized in Table 2. The MRD between two records is calculated by dividing the mean absolute difference by the mean profile, which gives an indication of bias whenever larger than the combined precisions of the two records – which is on the order of 1–2 %, given the large number of profiles included in the difference. The SD refers to the standard deviation of the mean difference, which gives an indication of the precision with which a bias is observed between the records. Note that the comparison statistics in Table 2 have been summarized over a limited pressure range going from 3 to 30 hPa in the tropics and from 5 to 50 hPa in the extratropics, which already holds more than 80–90 % of the total stratospheric column. These pressure limits have been used in earlier validation studies of stratospheric NO₂ profiles and thus facilitate reference to previous work.

Earlier validation studies indicate that SCIAMACHY limb profiles agree with MIPAS and GOMOS measurements to 10–20 % from 25 to 40 km (3 to 30 hPa), degrading to 30–50 % down to 15 km (100 hPa) (Bracher et al., 2005). The comparison against solar occultation measurements from HALOE, SAGE II and ACE-FTS gives an agreement typically within 20–30 % in the 20 to 40 km (3 to 50 hPa) altitude range (Bauer et al., 2012). The MIPAS NO₂ profiles agree with correlative ground-based and solar occultations from HALOE, SAGE II, POAM III and ACE-FTS to 15–30 % overall from 25 to 45 km (2 to 30 hPa) in non-perturbed conditions (i.e., in absence of solar proton events; Wetzel et al., 2007). Finally, the HIRDLS data quality document (Gille et al., 2012a) reports a preliminary agreement between HIRDLS and MIPAS within 20 % over the 3–30 hPa pressure range over most locations.

Our own findings, summarized on Table 2 and Fig. 5, confirm an agreement between SCIAMACHY and MIPAS within 15–20 % over the 3–50 hPa pressure range, excluding the lower tropical stratosphere (around 30 hPa) where SCIAMACHY consistently appears up to 30 % stronger than MIPAS. The agreement between HIRDLS and SCIAMACHY (or MIPAS) is verified within 20 % over extratropical latitudes, excluding the JJA and SON seasons over the Southern Hemisphere, where HIRDLS shows a positive bias of up to

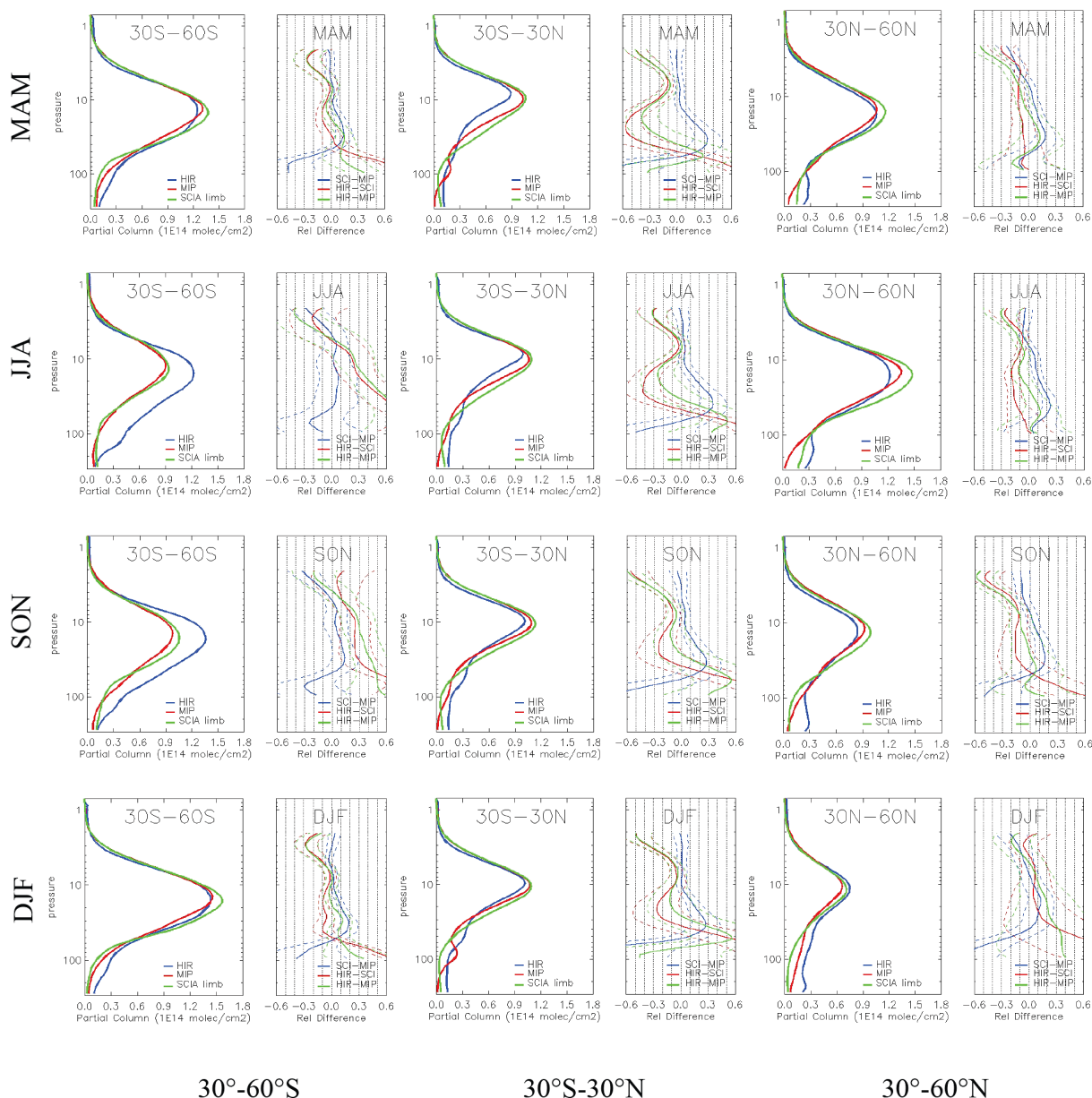


Figure 5. Partial column NO₂ profiles from HIRDLS (blue), MIPAS (red) and SCIAMACHY limb (green): means and mean relative differences over different latitude sectors (SH in the first column, tropical in the second column and NH in the third column) and seasons (MAM in the first row, JJA in the second row, SON in the third row and DJF in the fourth row).

60 % around and below peak NO₂ levels, and largest standard deviations in the differences that are indicative of instabilities in the radiance correction algorithm. Note that large SDs over the NH sector in DJF and over the SH sector in JJA and SON are in part also related to enhanced photocorrection factors. Over the tropics, the HIRDLS profiles show a negative bias of up to 30 % around and below the peak level relative to SCIAMACHY and MIPAS all year long.

Observations of stratospheric NO₂ below the 50 hPa pressure level (20 km) as provided by the limb instruments should contribute to the study of stratospheric aerosol effects (50 to

100 hPa) and UTLS exchange. However, this altitude domain is very sensitive to instrumental and photocorrection errors, and relative errors need to be interpreted more carefully.

In summary, we find very good and strong agreement between SCIAMACHY limb and MIPAS stratospheric NO₂ partial column profiles across the seasons and latitudes, with low mean relative differences and low standard deviations, reinforced by good (low mean relative difference) though not so strong (higher standard deviation) agreement to HIRDLS. The global average (min/max) relative difference between SCIAMACHY and MIPAS is 6 % (−17 to 33 %) from 3 to

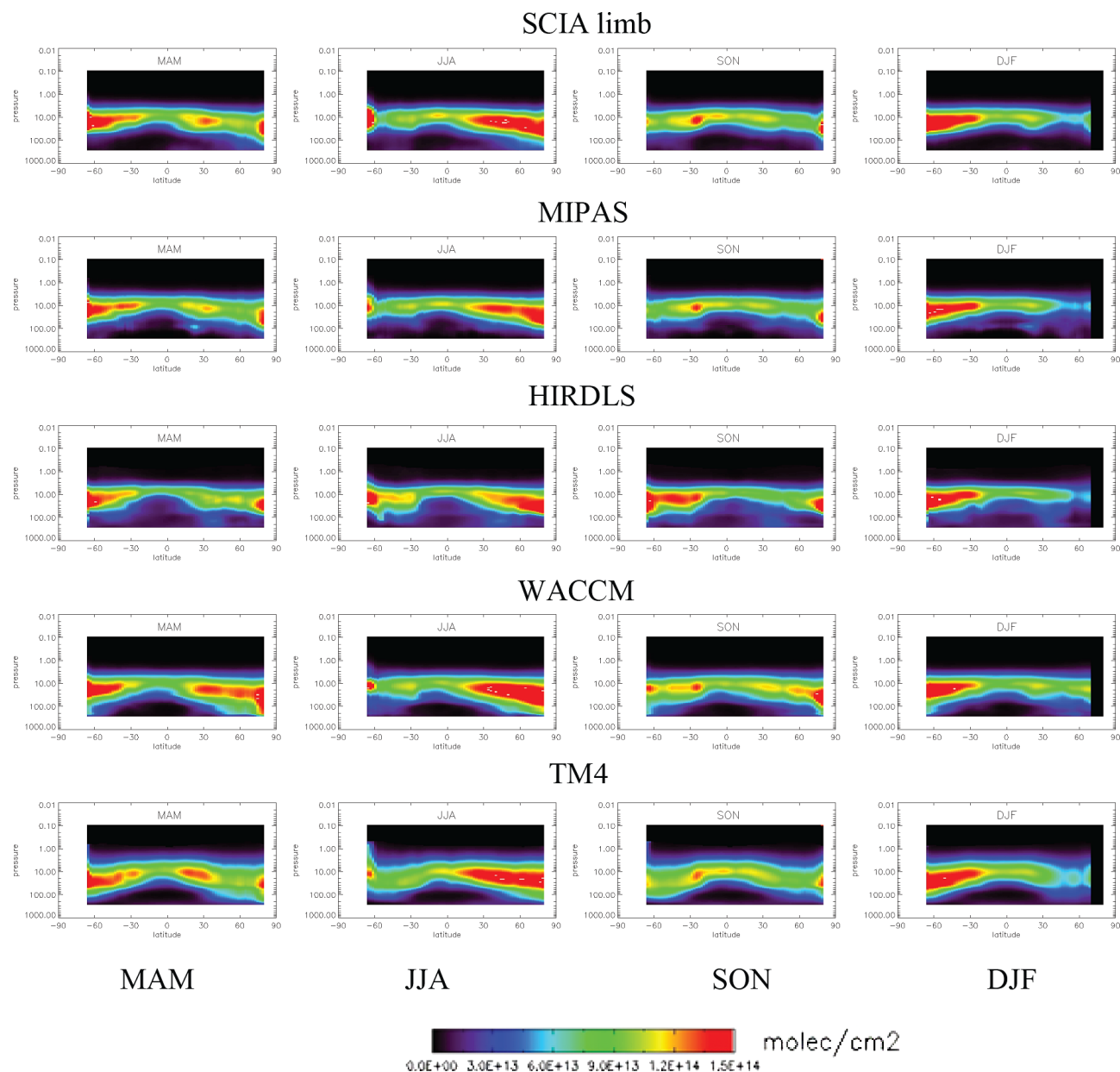


Figure 6. Seasonal mean stratospheric NO₂ partial column profiles for SCIAMACHY limb (first row), MIPAS (second row), HIRDLS (third row), WACCM (fourth row) and TM4 (fifth row) as a function of latitude.

30 hPa, determined with a global average standard deviation of 9%. Over the same pressure range, the global average (min/max) relative difference between HIRDLS and SCIAMACHY is −6% (−57 to 80%), determined with a global average standard deviation of 15%. The latest HIRDLS NO₂ profiles from version 7 seem to be up to 30% too low in the lower tropical stratosphere, and up to 60% too high in the Southern Hemisphere over the late summer and early fall seasons. The SCIAMACHY profiles appear to be up to 30% higher than MIPAS in the lower tropical stratosphere.

3.2 Model simulations

We introduce the partial column profiles of WACCM and the TM4 model (the latter after assimilation of the OMI total columns) and calculate their mean relative difference to the collection of limb observations, here represented by the SCIAMACHY limb data set. The comparison statistics are summarized in Fig. 7a.

We observe a general good agreement between WACCM and SCIAMACHY limb profiles over upper stratospheric levels and throughout the entire atmospheric depth in the

Table 2. Comparison statistics (MRD and SD) over 5–50 hPa (extratropics) and 3–30 hPa (tropics).

MAM	SH		EQ		NH	
	Mean (min/max) [%]	SD [%]	Mean (min/max) [%]	SD [%]	Mean (min/max) [%]	SD [%]
SCI-MIP	5 (–6/14)	6	8 (0/33)	7	4 (–16/18)	8
HIR-SCI	5 (–26/17)	10	–31 (–57/–10)	12	–9 (–21/–4)	10
HIR-MIP	0 (–27/15)	10	–23 (–39/–8)	13	–5 (–37/13)	13
JJA	Mean (min/max) [%]	SD [%]	Mean (min/max) [%]	SD [%]	Mean (min/max) [%]	SD [%]
SCI-MIP	2 (–14/8)	19	9(1/32)	7	8 (–6/23)	6
HIR-SCI	25 (–20/80)	24	–22 (–42/–3)	12	–14 (–21/–6)	7
HIR-MIP	27 (–34/76)	26	–14 (–26/0)	15	–6 (–26/12)	9
SON	Mean (min/max) [%]	SD [%]	Mean (min/max) [%]	SD [%]	Mean (min/max) [%]	SD [%]
SCI-MIP	4 (–17/15)	12	7 (0/27)	7	4 (–8/16)	9
HIR-SCI	22 (5/50)	17	–19 (–39/–9)	13	–16 (–42/4)	15
HIR-MIP	26 (–11/48)	19	–11 (–39/7)	15	–11 (–51/7)	17
DJF	Mean (min/max) [%]	SD [%]	Mean (min/max) [%]	SD [%]	Mean (min/max) [%]	SD [%]
SCI-MIP	6 (–2/17)	6	7 (0/27)	7	2 (–17/13)	13
HIR-SCI	–8 (–29/2)	8	–16 (–36/–4)	16	11 (–5/52)	31
HIR-MIP	–1 (–28/13)	8	–9 (–34/11)	16	13 (–17/36)	33

tropics, typically within 30 %. However, the WACCM peak NO₂ densities over the extratropics appear to be located too low in altitude (lower by about 5–10 hPa) and span too broad a pressure range compared to the limb instrument observations, with large positive biases (over 100 %) in the lower stratosphere that become particularly acute in the springtime and over northern latitudes. The comparison between TM4 and the limb data set conveys a similar portrait: good agreement between model and observations throughout the entire atmospheric depth in the tropics, with model peak NO₂ densities that are too low in altitude and too broad in extent in the extratropics, producing large positive biases in the lower stratosphere. The assimilated TM4 model also suffers from a persistent positive bias at upper stratospheric levels across latitudes and seasons – which is likely related to the HNO₃ nudging scheme and fixed NO_x mixing ratio above 10 hPa.

We conclude that the mechanisms of NO₂ production and transport over the equatorial NO_y production zone appear to be reasonably well represented in WACCM, although there may be issues with chemistry and/or transport into the extratropical lower stratosphere, particularly in the springtime (both hemispheres) and over the Northern Hemisphere, as illustrated in Fig. 7b.

3.3 Nadir measurements

At this point we introduce the stratospheric columns derived from nadir instruments into the comparison. Recall that all data sets have been photocorrected to HIRDLS local solar times and that stratospheric columns are integrated to 287 hPa. The average difference in stratospheric

columns calculated using a lower integration level of 287 hPa and the dynamical tropopause pressure is about 0.05×10^{15} molecules cm^{–2} over the tropics and zero elsewhere.

The seasonally averaged stratospheric NO₂ columns measured by nadir instruments are shown in Fig. 8, along with their limb and model counterparts. The stratospheric NO₂ columns are characterized by a tropical minimum over the equatorial NO_y production zone, where total nitrogen is subject to upward and poleward transport. Figure 9a illustrates the extratropical seasonal cycle marked by winter minima and summer maxima, characterized by an amplitude that increases with latitude. Similar to the diurnal NO₂ variation, the seasonal evolution of NO_x is explained by the steady-state concentration of N₂O₅ (Solomon and Garcia, 1983) after balance between nighttime formation and daytime destruction. As the amount of daily photolysis decreases over winter, NO_x begins to store into inactive N₂O₅ reservoirs, but also into HNO₃, ClONO₂ and BrONO₂, as polar winter conditions set heterogeneous processes in motion, which results in a decrease of NO_x columns. Conversely, the photolytically driven release of reservoirs over the summer season results in an increase of NO_x columns into the summer hemisphere. Asymmetries between the NH and SH distributions, such as the larger winter abundances observed in Fig. 9a in the Southern Hemisphere, should be attributed to first order to the slight asymmetry in the HIRDLS LST-latitude curve (Fig. 3). Note that the dependence of the HIRDLS local solar time on latitude leaves observations over the Southern Hemisphere more exposed to nighttime conditions during the winter season. The physical basis behind inter-hemispheric asymmetries in stratospheric NO₂ distributions

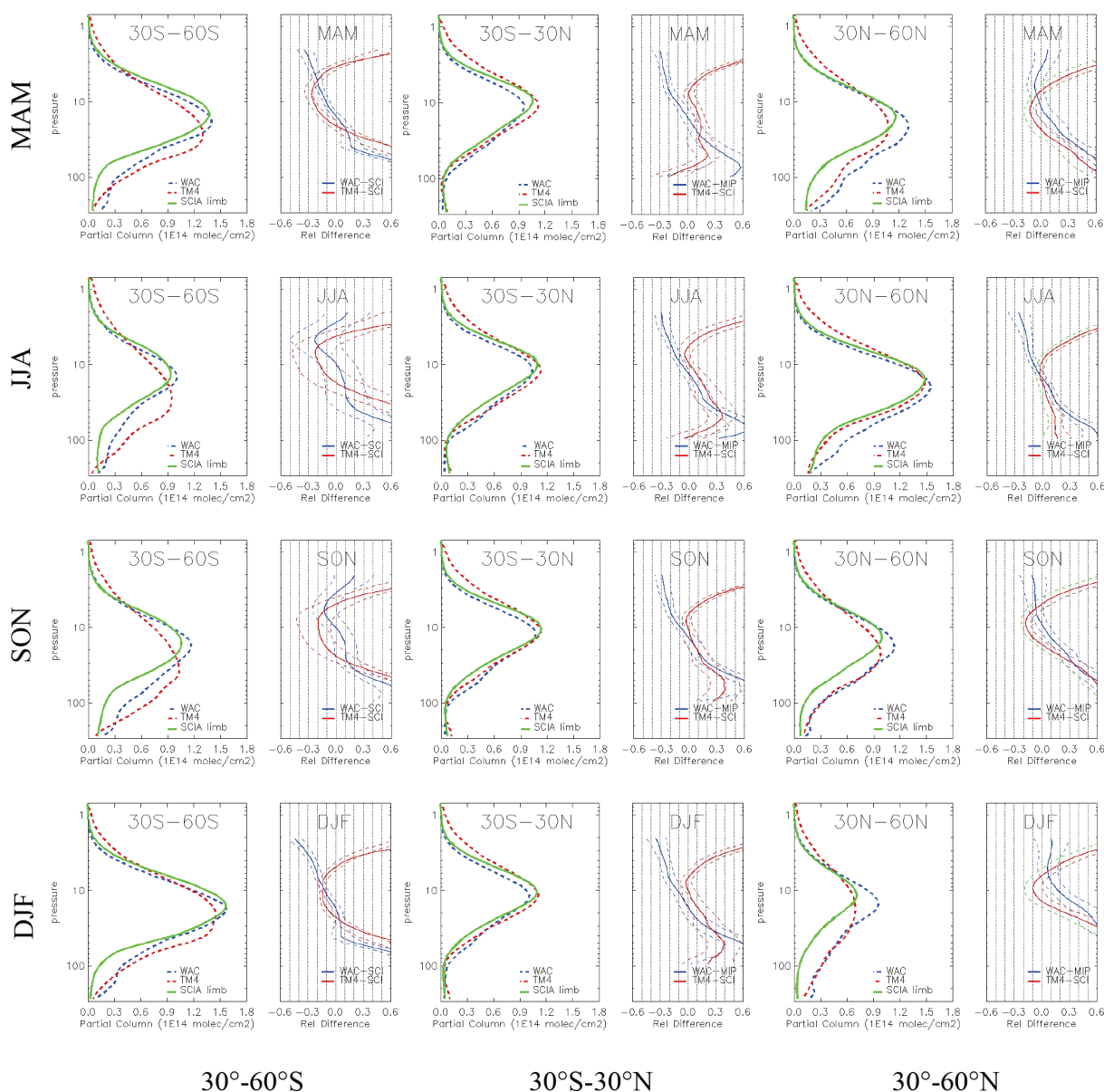


Figure 7. Partial column NO₂ profiles from SCIAMACHY (green), WACCM (dashed blue) and TM4 (dashed red): means and mean relative differences over different latitude sectors (SH in the first column, tropical in the second column and NH in the third column) and seasons (MAM in the first row, JJA in the second row, SON in the third row and DJF in the fourth row).

has been attributed to dynamic and radiative conditions arising from reduced wave driving in the Southern Hemisphere winter (Solomon et al., 1984; Rosenlof, 1995; Dirksen et al., 2011).

The presence of a strong seasonal cycle in the extratropics makes tropical latitudes better suited to the study of long-term trends, although natural variability also plays a role. The evolution of stratospheric NO₂ columns over the Equator (middle panel in Fig. 9a) is subject to a small annual cycle with minimum columns in the northern winter (January) related to strong updrafts from the wave-driven circulation.

Figure 9b shows the altitude cross section of stratospheric NO₂ columns over the Equator, where a small negative QBO signal may be appreciated around January 2007 (Dirksen et al., 2011). Here a negative quasi-biennial oscillation (QBO) phase related to a predominant easterly shear zone is acting, along with the annual winter updraft, to advect NO_x-poor air from below (Zawodny and McCormick, 1991). The presence of natural variability makes the combination of records from multiple satellite data sets (e.g., GOME, SCIAMACHY, OMI) very appealing for the study of long-term trends.

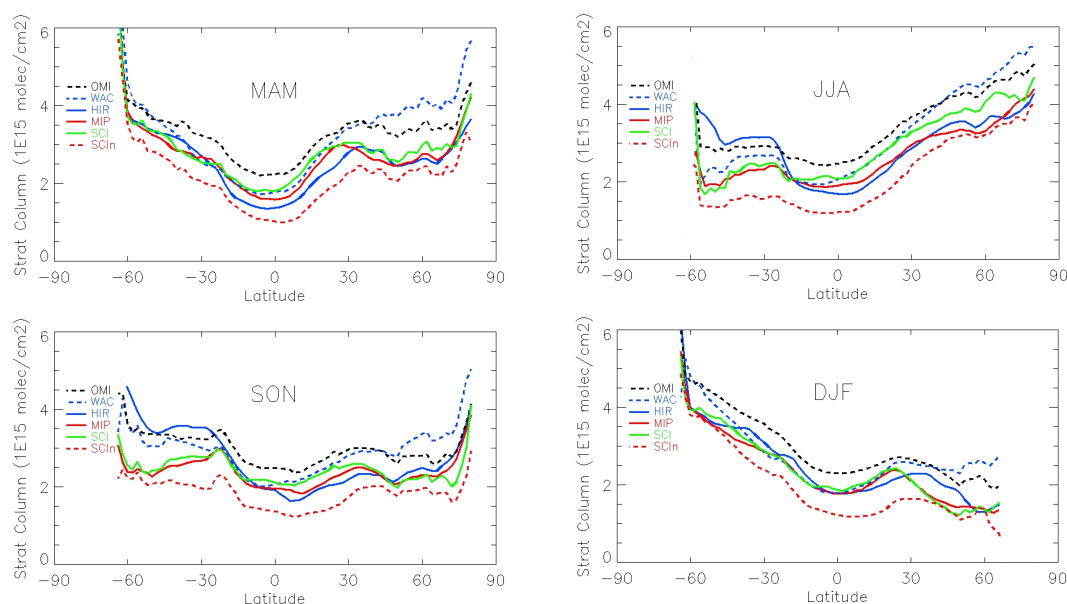


Figure 8. Seasonally averaged (MAM, JJA, SON and DJF) stratospheric NO₂ columns from SCIAMACHY limb (green), MIPAS (red), HIRDLS (blue), WACCM (dashed blue), SCIAMACHY nadir (SCIn, dashed red) and OMI (dashed black) integrated down to 287 hPa.

Focusing solely on the limb collection formed by SCIAMACHY limb, MIPAS and HIRDLS records in Fig. 8, we observe a very close agreement across latitudes and seasons, with the exception of HIRDLS over southern latitudes in the JJA and SON seasons, which we already singled out as anomalous back when we examined the partial column profiles in Fig. 5. This close agreement suggests that we can define a limb reference for stratospheric NO₂ columns that combines SCIAMACHY limb, MIPAS and HIRDLS records, but excludes HIRDLS data over the southern latitudes during the JJA and SON seasons. A summary of the mean differences of limb, nadir and model stratospheric NO₂ records to the limb reference is shown in Tables 3 and 4. The limb reference agrees with each of its constitutive data sets to within 0.25×10^{15} molecules cm⁻², and the fact that it is formed using records derived from entirely independent techniques (from infrared emission to solar UV/VIS scattering) lends it additional solidity. Having such a consistent reference from the limb instruments allows us to make inferences about the quality of the other data sets.

For instance, the stratospheric NO₂ columns from WACCM match the limb observations neatly over the tropics, as seen in Tables 3 and 4, but are too large in the extratropics, particularly in the Northern Hemisphere, by as much as 1.0×10^{15} molecules cm⁻² (35 %) relative to the limb reference. Mean relative biases from SCIAMACHY nadir to the limb reference over {SH, Eq, NH} are $\{-0.5, -0.7, -0.4\} \times 10^{15}$ molecules cm⁻², with a small seasonal cycle in the tropics and NH of 0.15×10^{15} molecules cm⁻², and a stronger seasonal signal of 0.3×10^{15} molecules cm⁻² in the SH, featuring largest discrepancies in JJA and smallest in DJF. Mean

relative biases from OMI to the limb reference over {SH, Eq, NH} are $\{0.7, 0.5, 0.6\} \times 10^{15}$ molecules cm⁻², also with a small seasonal cycle in the tropics and NH, and a larger seasonal cycle of 0.3×10^{15} molecules cm⁻² in the SH, featuring largest discrepancies in SON and smallest in MAM over the Southern Hemisphere (reversed over the NH). The relative bias between the SCIAMACHY nadir and OMI data sets over {SH, Eq, NH} is $\{1.1, 1.2, 1.0\}$ molecules cm⁻² or about 30–50 %.

The offset between SCIAMACHY limb and SCIAMACHY nadir retrievals has been observed before by Beirle et al. (2010) and Hillboll et al. (2013). The latter noted that the limb–nadir bias in SCIAMACHY showed a seasonally and latitudinally dependent pattern similar to that shown here, with a seasonal cycle in the Southern Hemisphere of about 0.3×10^{15} molecules cm⁻² and smallest discrepancies over the austral summer. Their results indicate that the columns from SCIAMACHY limb (same IUP Bremen retrieval version 3.1 as is used here) are higher than those from SCIAMACHY nadir (from IUP Bremen retrieval, different from the KNMI-BIRA algorithm used here) by about 0.2 – 0.4×10^{15} molecules cm⁻² over the tropics, implying that the SCIAMACHY nadir stratospheric columns from the IUP Bremen retrieval are higher than those derived from KNMI-BIRA by about 0.3 – 0.4×10^{15} molecules cm⁻². The difference could be arising from the utilization of different retrieval configurations in the generation of nadir columns.

Boersma et al. (2008) also noted an offset in normalized total slant columns between OMI and SCIAMACHY nadir of 0.6×10^{15} molecules cm⁻² for August 2006 – before photocorrection, which is about one half of what we observe

Table 3. Mean stratospheric column differences to limb reference (in 10^{15} molecules cm^{-2} , italicized if larger than 0.25). The latitude sectors correspond as follows: SH = 30–60° S; Eq = 30° S–30° N; and NH = 30–60° N.

	MAM			JJA			SON			DJF		
	SH	Eq	NH	SH	Eq	NH	SH	Eq	NH	SH	Eq	NH
SCIA limb	−0.02	0.19	0.10	0.03	0.11	0.22	0.06	0.07	−0.01	0.04	0.03	−0.16
MIP	−0.07	0.05	−0.09	−0.03	−0.11	−0.22	−0.06	−0.07	−0.01	−0.12	−0.02	−0.08
HIRDLS	0.09	−0.24	−0.01	<i>1.11</i>	−0.14	−0.10	<i>1.06</i>	−0.06	−0.01	0.08	−0.02	0.24
WACCM	<i>0.31</i>	0.15	<i>1.01</i>	<i>0.32</i>	0.12	<i>0.69</i>	<i>0.64</i>	0.13	<i>0.66</i>	<i>0.31</i>	0.02	<i>0.80</i>
SCIA nadir	−0.52	−0.64	−0.41	−0.64	−0.79	−0.46	−0.42	−0.72	−0.38	−0.32	−0.65	−0.28
OMI	<i>0.47</i>	<i>0.61</i>	<i>0.72</i>	<i>0.79</i>	<i>0.51</i>	<i>0.63</i>	<i>0.80</i>	<i>0.47</i>	<i>0.56</i>	<i>0.66</i>	<i>0.46</i>	<i>0.64</i>

Table 4. Same as Table 3, but in percent (%) relative to the limb reference.

	MAM			JJA			SON			DJF		
	SH	Eq	NH	SH	Eq	NH	SH	Eq	NH	SH	Eq	NH
SCIA limb	−0.6	9.3	3.7	1.2	4.8	6.4	2.2	3.2	0.5	1.3	1.5	−9.7
MIP	−2.3	2.2	−3.4	−1.2	−4.8	−6.4	−2.2	−3.2	−0.5	−3.5	−0.9	−4.6
HIRDLS	3.0	−11.6	−0.2	<i>50.6</i>	−6.5	−2.8	<i>41.5</i>	−2.5	−0.1	2.2	−0.6	14.3
WACCM	9.9	7.1	<i>37.5</i>	<i>14.8</i>	5.3	<i>20.0</i>	<i>25.2</i>	5.6	<i>28.7</i>	8.8	1.0	<i>48.4</i>
SCIA nadir	−16.4	−30.4	−15.3	−29.0	−34.7	−13.4	−16.4	−31.5	−16.4	−9.2	−29.7	−16.6
OMI	<i>15.0</i>	28.9	26.4	<i>35.9</i>	22.2	<i>18.4</i>	<i>31.1</i>	20.5	<i>24.3</i>	<i>18.9</i>	<i>21.3</i>	<i>38.6</i>

here (they used older retrieval versions for OMI – DOMINO version 0.9 – and SCIAMACHY nadir – TM4NO2A version 1.04 – in that study) – and attributed the discrepancy to differences in the reference solar spectrum used for spectral fitting. It becomes clear that stratospheric NO₂ columns derived from nadir instruments like SCIAMACHY and OMI show marked seasonally and latitudinally dependent biases that are sensitive to the retrieval configuration used to generate them (i.e., wavelength calibration, absorption cross sections for NO₂, spectral fit window width, number of interfering species, spectral resolution, solar reference spectra, ring spectra, etc.).

At this point, an examination of the role of the NDACC ground-based stations as the validation sources emerges. Dirksen et al. (2011) determined that stratospheric NO₂ columns from ground-based (UV/VIS and FTIR) and satellite nadir OMI (DOMINO version 1.0) retrievals at various NDACC stations (including Jungfraujoch, Izana and Sodankyla) agreed to within 0.3×10^{15} molecules cm^{-2} . Similarly, Hendrick et al. (2012) did not find any significant biases between ground-based (UV/VIS and FTIR) and satellite nadir UV/VIS observations of stratospheric NO₂ for the 1996–2009 period (using overlapping GOME, SCIAMACHY (version 1.10) and GOME II records) at Jungfraujoch (46.5° N) over the year 2005. The fact that the NDACC could not identify a seasonally or latitudinally dependent bias in either SCIAMACHY nadir or OMI slant columns remains unexplained. As a further matter, Wetzel et al. (2007) did not find any significant biases between the ground-based (UV/VIS) and the MIPAS record at Jungfraujoch over the

year 2003. Wetzel et al. (2007) conducted comparisons of MIPAS against the entire NDACC UV/VIS network from 80° S to 80° N to conclude that the agreement fell within the accuracy limit of the comparison method. Additional comparisons against NDACC ground-based FTIR records in Kiruna and Harestua revealed a degree of seasonality in the relative differences, with a ground-based FTIR daytime record that appeared up to 0.5×10^{15} molecules cm^{-2} larger than MIPAS during the NH summer. Current efforts to anchor satellite measurements to ground-based references do not appear precise enough for a clear picture to emerge. It is in this light that we opt to lean to the side of consistency among large but independent data sets, like those from the satellite limb collection, as a validation source.

In the following, we argue on two important points: (1) that additive biases in nadir stratospheric columns are not expected to affect the tropospheric column significantly and (2) that biases in nadir stratospheric vertical columns cannot be attributed to errors in the air mass factor, so they must arise from errors in the fitted slant column densities.

Point 1 – effects on tropospheric columns

Recall that the assimilation adjustment required for the formation of the nadir stratospheric column is proportional to the product of the averaging kernel and the a priori trace gas profile as in Eq. (10). A look at the typical averaging kernel and trace gas profiles over clean NO₂ backgrounds ($N_{\text{v, trop}} < 1 \times 10^{15}$ molecules cm^{-2}) under cloudy and clear-sky conditions is given in Fig. 10. Note that the sensitivity to

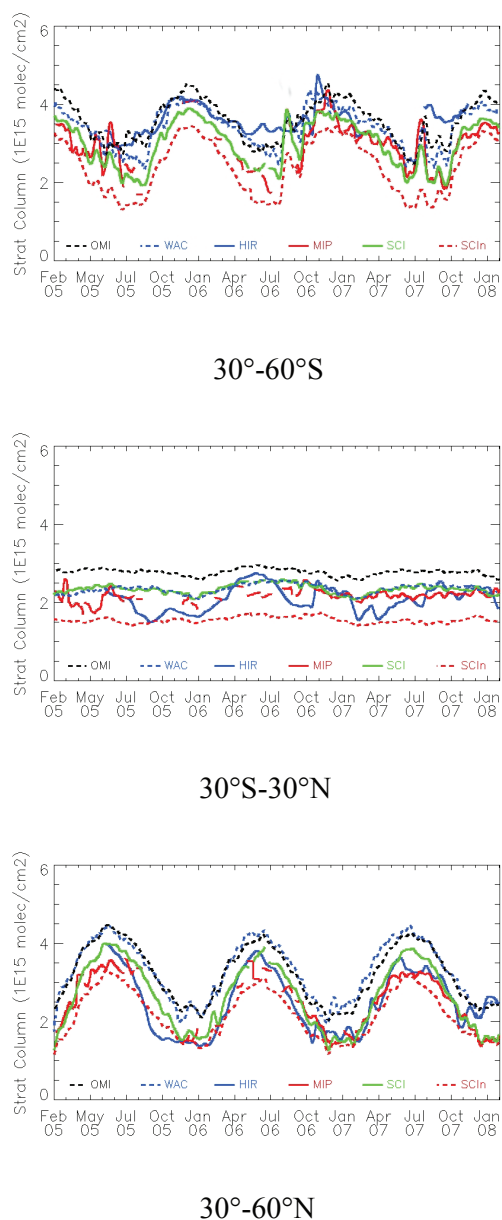


Figure 9a. Time trends in stratospheric columns of NO₂ columns (SH in top panel, tropics in middle panel, NH in bottom panel) from SCIAMACHY limb (green), MIPAS (red), HIRDLS (blue), WACCM (dashed blue), SCIAMACHY nadir (dashed red) and OMI (dashed black) integrated down to 287 hPa.

NO₂ is strongly reduced in the troposphere. The difference between the left and middle panels in Fig. 10 is explained by the temperature correction factor $c[T(z)]$. The right panel in Fig. 10 shows that assimilation adjustments are distributed mainly above the 500 hPa level. Under average conditions, an increase of 100 % in the stratospheric component forced by assimilation (i.e., $\alpha = 1.0$ in Eq. 10) will translate into an approximately 50 % increase in the clean tropospheric component by virtue of the reduced tropospheric sensitivity

encoded in the kernel constraint. Therefore, one would expect an average positive bias of 0.1×10^{15} molecules cm^{-2} in the tropospheric component in response to a stratospheric bias of 100 % forced by observations, assuming a clean background with average $N_{\text{v, trop}} = 0.2 \times 10^{15}$ molecules cm^{-2} . This amount is rather inconsequential, but note that larger “forced tropospheric biases” could arise locally over clean areas with large NO₂ amounts in the upper troposphere, as the tropospheric NO₂ background reaches the assimilation top of 0.5×10^{15} molecules cm^{-2} (i.e., the approximate level beyond which the Kalman filter will start rejecting observations for having too large a tropospheric component).

In summary, biases in the slant column lead to biases in the stratospheric NO₂ column without affecting the tropospheric column, because only observations over remote/unpolluted areas are used to assimilate the stratospheric model field. This explains why no significant biases are observed in clean tropospheric NO₂ backgrounds between OMI and SCIAMACHY nadir data sets (see right panel on Fig. 11, with a median difference of 0.04×10^{15} molecules cm^{-2} in the tropospheric background). Because biases in the nadir stratospheric column are advected by the chemical transport model over the polluted regions, one should therefore not expect any significant effect on polluted tropospheric columns, as long as the bias in the slant column is additive.

Point 2 – influence of the stratospheric air mass factor

The estimation of nadir stratospheric columns from slant column retrievals ($N_{\text{v}} = N_{\text{s}}/M$) involves a number of assumptions encoded in the air mass factor such as the scattering sensitivity profile $m(z)$, the model gas profile $n_{\text{v}}(z)$ or the correction to temperature sensitivity $c[T(z)]$. A cursory look at the effects of these assumptions on stratospheric columns should convince us that uncertainties around a priori are of small import, and that biases in vertical columns can be directly mapped to biases in the fitted slant column densities. The argument revolves around the fact that most of the signal in a slant column over a clean background is stratospheric in origin. The stratospheric slant column is corrected for viewing geometry and temperature sensitivity via the stratospheric air mass factor, but the amplitude of these corrections is not (and cannot be) as large as needed to explain the seasonally and latitudinally dependent patterns of bias observed.

Recall that the normalized total slant column ($N_{\text{s}}/M_{\text{geo}}$), where normalized refers to scaled by the geometric AMF, can be split into stratospheric and tropospheric components as

$$N_{\text{s}}/M_{\text{geo}} = (N_{\text{v, strat}} \cdot M_{\text{strat}} + N_{\text{v, trop}} \cdot M_{\text{trop}})/M_{\text{geo}}. \quad (13)$$

As shown in Fig. 11, the normalized tropospheric slant column ($N_{\text{s, trop}}/M_{\text{geo}}$) features a statistical mode at 0.13×10^{15} molecules cm^{-2} representative of a clean NO₂ background, which amounts to 5 % of the total slant column. Thus, a tropospheric source may on average be safely discarded as a cause of stratospheric bias. Exceptions to this rule

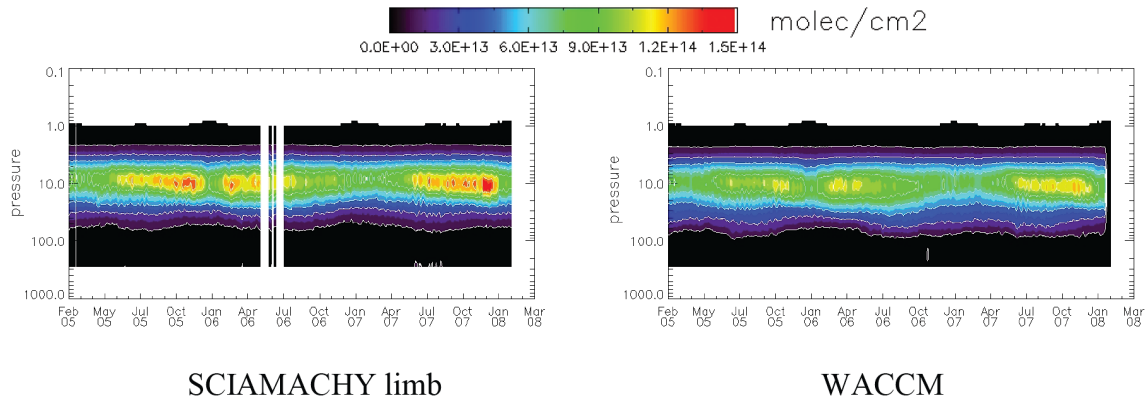


Figure 9b. Time trends in stratospheric NO₂ partial column profiles at Equator from SCIAMACHY (left plot) and WACCM (right plot).

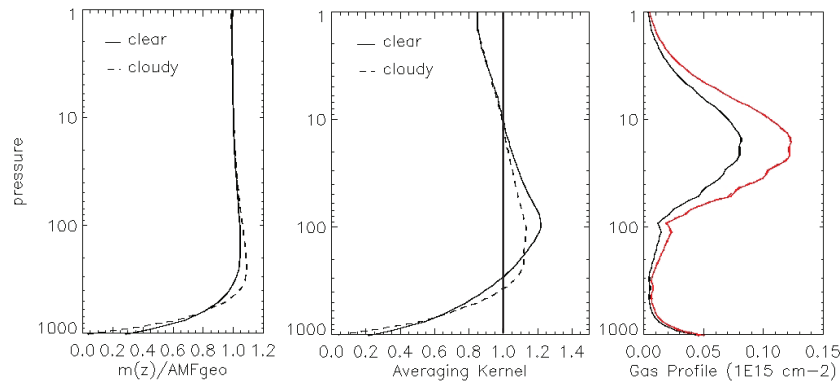


Figure 10. Normalized scattering sensitivity $m(z)/M_{\text{geo}}$, averaging kernel $A(z)$ and vertical distribution of assimilation increments in clear-sky (continuous line, cloud radiance fraction CRF < 25 %) and cloudy (dashed line, cloud radiance fraction CRF > 75 %) unpolluted conditions on 21 March 2005 (global averages), following Eq. (10). On the right panel, the black and red lines refer to before and after adjustment, respectively.

may occur over areas with significant differences between a priori and observed tropospheric columns. A characteristic error signature would arise in this case that would make this easy to identify.

In order to be mapped into a vertical column, the stratospheric slant column is scaled by the stratospheric air mass factor M_{strat} , which contains a correction for scattering sensitivity, M_0 , and another for temperature sensitivity, $c(T_{\text{eff}})$. From Eq. (2),

$$M_{\text{strat}} = c(T_{\text{eff}}) \cdot M_0. \quad (14)$$

The scattering air mass factor M_0 in the stratosphere is defined as

$$M_0 = \sum_{\text{strat}} m(z) \cdot n_{v0}(z) / N_{v0}, \quad (15)$$

where $N_{v0} = \sum_{\text{strat}} n_{v0}(z)$, and the correction for temperature sensitivity $c(T_{\text{eff}})$ from Eq. (3) is a function of the column effective temperature T_{eff} , which is a weighted column average

expressed as (Chance, 2002)

$$T_{\text{eff}} = \sum_{\text{strat}} T(z) \cdot m(z) \cdot n_{v0}(z) / \sum_{\text{strat}} m(z) \cdot n_{v0}(z). \quad (16)$$

Since the normalized scattering sensitivity $m(z)/M_{\text{geo}}$ is close to unity everywhere in the stratosphere (see left panel on Fig. 10), the normalized scattering air mass factor M_0 will also approximate unity in the stratosphere (see Fig. 12), and the stratospheric air mass factor M_{strat} will be solely dependent on the shape of the a priori temperature and gas profiles (via the effective column temperature T_{eff}).

Figure 12 shows the seasonally averaged stratospheric air mass factors, split into their scattering air mass M_0 and temperature correction $c(T_{\text{eff}})$ factors as a function of latitude. The normalized scattering air mass factor M_0 lies generally within 1 % of a flat global annual mean – with an absolute value about 2–3 % larger than the geometric AMF, reflecting that only a small fraction of the light is scattered within the stratosphere. The amplitude of the stratospheric temperature correction $c(T_{\text{eff}})$, which dominates the seasonal and latitudinal variability of the stratospheric AMF, lies generally

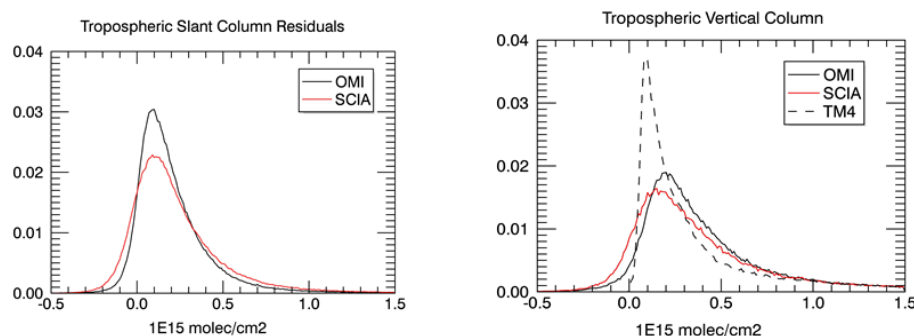


Figure 11. Histogram of global tropospheric NO₂ columns from OMI and SCIAMACHY nadir (normalized slant column N_s on the left, and vertical column N_v on the right) for 2005 with CRF < 50 % – uncorrected for diurnal variation. The OMI and SCIA global median normalized slant column N_s is 0.20 and 0.21 (0.13 and 0.13 mode) $\times 10^{15}$ molecules cm^{-2} , respectively. The OMI and SCIA global median vertical column N_v is 0.30 and 0.26 (0.20 and 0.15 mode) $\times 10^{15}$ molecules cm^{-2} , respectively. The median tropospheric column for the TM4 model is 0.21 (0.09 mode) $\times 10^{15}$ molecules cm^{-2} .

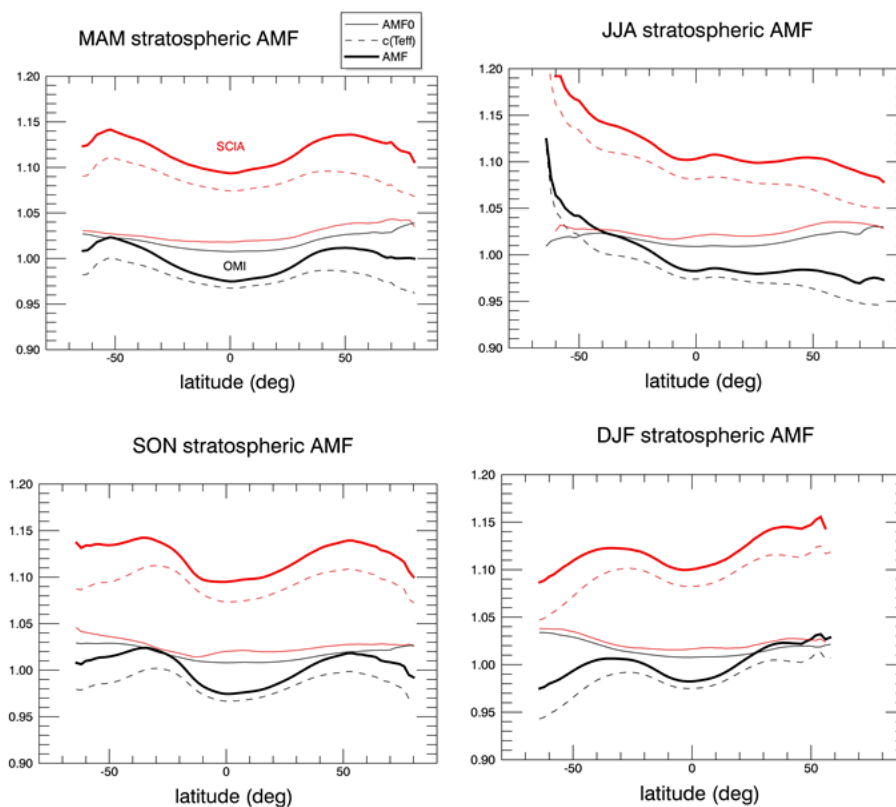


Figure 12. Average (MAM, JJA, SON and DJF) stratospheric air mass factors for 2005 plotted as a function of latitude for OMI (black) and SCIAMACHY (red) with components split into normalized scattering air mass factor M_0 (thin continuous), temperature correction factor (dashed) and total stratospheric air mass factor M_{strat} (thick continuous).

within 5 % of a flat annual global mean – with absolute values of 1.10 for SCIAMACHY and 0.99 for OMI, which only reflect the different reference temperatures chosen for the spectral fit retrieval, namely $T_{\text{ref}} = 243$ K for SCIAMACHY nadir and $T_{\text{ref}} = 220$ K for OMI. The temperature correction proves largely insensitive to uncertainties in the a priori gas and temperature profiles. The ECMWF temperature profiles

are estimated to be accurate up to a few degrees (Knudsen, 2003), leading to errors of approximately 1 % in the temperature correction. Likewise, replacing the a priori gas profile with a reference gas profile from the limb collection will not change the effective column temperature by more than 2–3 K, which in turn will not affect the temperature correction $c(T_{\text{eff}})$ by more than 1 % in the OMI case and 1.5 % in the

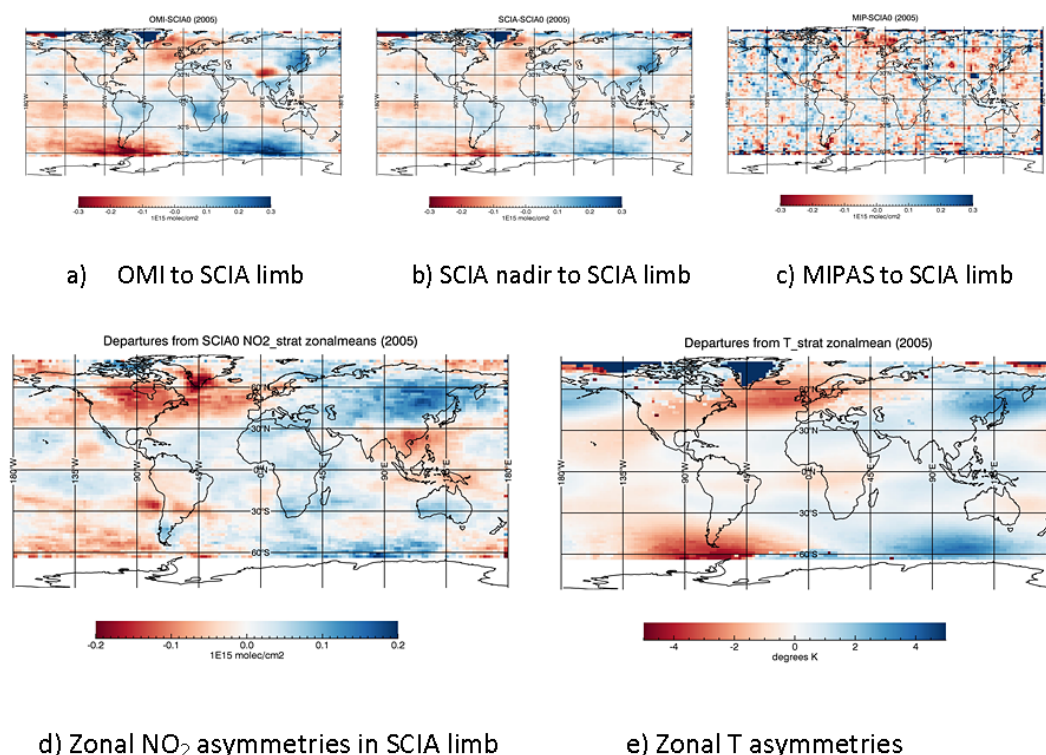


Figure 13. Longitudinal error signatures: annual differences in stratospheric NO₂ for 2005 between (a) OMI and SCIAMACHY limb, (b) SCIAMACHY nadir and SCIAMACHY limb and (c) MIPAS and SCIAMACHY limb, after removal of a latitudinally dependent bias. The lower plot shows geophysical departures of (d) stratospheric NO₂ columns and (e) temperatures from the annual zonal means.

SCIAMACHY nadir case. This also attests to the fact that a suboptimal representation of the stratospheric NO₂ profile like that provided by TM4 is enough for assimilation purposes.

In summary, the fact that the tropospheric contribution to the slant column makes up on average 5 % of the total column over a clean background, the normalized scattering air mass factor M_0 in the stratosphere lies within 1 % of a flat global annual mean centered around 1.02–1.03 for OMI and SCIAMACHY, the temperature correction factor lies within 5 % of a flat global annual mean centered around 0.99–1.10 for OMI and SCIAMACHY and that neither component of the stratospheric air mass factor proves sensitive to uncertainties in a priori gas and temperature profiles leaves little room to think that the stratospheric AMF could play any significant role in the biases observed, which reach up to 20–30 % in the OMI and SCIAMACHY nadir cases. Since none of the factors that mediate the transformation from total slant to stratospheric vertical columns can explain the biases observed in the nadir records, we infer that these must arise directly from errors in the fitted slant column densities. Indeed, the apparent offset in the OMI stratospheric NO₂ columns is currently under investigation and has been preliminarily traced to spectral differential optical absorption spectroscopy (DOAS) fit sensitivities to wavelength calibration,

liquid water and O₂–O₂ contributions (Jos van Geffen, personal communication, 2013). Independent adjustments to the OMI spectral fit algorithm report decrements in vertical column densities as large as 20–40 % (Krotkov et al., 2014), which are consistent with the differences that we observe to the limb reference.

Zonal asymmetries

A look at the longitudinal signatures of nadir-to-limb discrepancies left after removing a latitudinally dependent bias such as depicted in Fig. 8 may help throw additional information about the nature of stratospheric (or slant column) biases in the nadir records. The top panels in Figs. 13–14 show that the strongest zonal asymmetries in the nadir-to-limb difference plots correspond to a wave-one pattern located poleward of 45° with an amplitude of $\pm[0.15, 0.30] \times 10^{15}$ molecules cm⁻² for SCIAMACHY and OMI. This pattern appears to be strongest in the spring months (during the breaking up of the winter vortex, MAM in NH and SON in SH) at locations where departures from the zonal mean temperature are largest (up to ± 4 K from the annual mean on the lower right panel in Fig. 13). The correlation between the longitudinal variability in nadir-to-limb discrepancies and the departures of temperature from the zonal mean translates into a sensitivity to stratospheric effective column

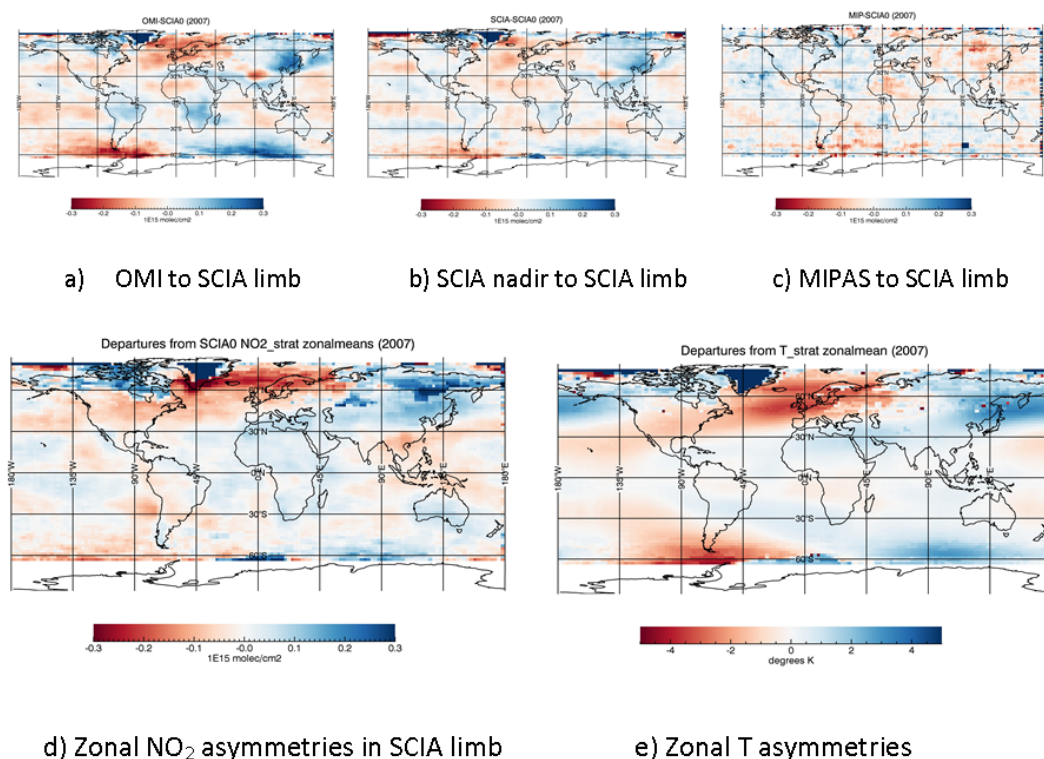


Figure 14. Same as Fig. 13 but for 2007. MIPAS sampling is denser in 2007, so the differences between MIPAS and SCIAMACHY limb come out cleaner.

temperature of $2\% \text{ K}^{-1}$ for SCIAMACHY and OMI vertical columns, which is several times larger than the temperature sensitivity of $0.5\% \text{ K}^{-1}$ that arises from the NO₂ cross-section temperature dependence according to Boersma et al. (2004) or $0.3\% \text{ K}^{-1}$ according to Bucselá et al. (2013).

One aspect that may partly explain the temperature-correlated signatures observed in Fig. 13a and b is the photocorrection, which assumes that the factors that control the diurnal NO₂ cycle, such as stratospheric temperature, do not have a longitudinal dependency. Model studies indicate that vertical NO₂ columns have a sensitivity of around $0.5\% \text{ K}^{-1}$ to changes in stratospheric temperature – as increasing temperatures increase NO₂ columns (see panel d in Fig. 13) while reducing the diurnal variation (Cook and Roscoe, 2009). But the photocorrection alone cannot justify the differences between the SCIAMACHY nadir and limb records seen in Fig. 13b, since both data sets are in this case multiplied by the same zonally averaged photocorrection factor. The map of longitudinal anomalies between SCIAMACHY limb and MIPAS (see Fig. 13c), though somewhat noisier due to poorer sampling, does not give indication of any temperature-correlated difference. The small differences between MIPAS and SCIAMACHY limb anomalies confirm the longitudinal consistency of the limb reference and suggest the presence of temperature-correlated errors in the nadir data sets.

4 Summary and conclusions

Our comparison of stratospheric NO₂ profiles from various satellite limb records confirms an agreement within 15–20 % over the 3–50 hPa pressure range between MIPAS and SCIAMACHY over the 2005–2007 period, excluding the lower tropical stratosphere (around 30 hPa) where SCIAMACHY limb partial column profiles consistently appear up to 30 % larger than MIPAS. The agreement between HIRDLS and SCIAMACHY limb (and MIPAS) profiles is confirmed within 20 % over extratropical latitudes, excluding the late summer (JJA) and early fall (SON) season over the Southern Hemisphere, where HIRDLS is affected by a positive bias of about 60 % at and below peak NO₂ levels. Over the tropics, HIRDLS shows a negative bias of up to 30 % at and below peak NO₂ levels all year long, which is likely attributable to shortcomings of the radiance correction algorithm. Overall, we find an accurate and precise agreement between MIPAS and SCIAMACHY limb partial column NO₂ profiles across latitudes and seasons, with mean relative errors between –17 and 33 % and an average standard deviation of 9 %, reinforced by accurate though not so precise agreement to HIRDLS, with mean relative errors between –57 and 52 % (excepting the JJA and SON sectors in SH) and an average standard deviation of 15 %.

The comparison of stratospheric NO₂ profiles from the WACCM and TM4 model simulations and limb observations reveals a consistent portrait: there is good agreement between modeled and observed partial column profiles throughout the atmosphere over tropical latitudes (with mean relative errors within 30 %), but model NO₂ profiles tend to exhibit large positive biases (up to 100 %) in the extratropical lower stratosphere, with peak NO₂ densities that are generally low by 5–10 hPa and too broad in extent relative to limb observations, particularly over the northern latitudes, suggesting an incomplete understanding of the factors that regulate lower stratospheric extratropical NO₂ densities in these models.

A conclusion central to this paper is that a reference for stratospheric NO₂ columns may be defined based on the strong agreement between SCIAMACHY limb, MIPAS and HIRDLS records, good to within 0.25×10^{15} molecules cm⁻². Previous validation work using ground-based observations does not seem consistent or precise enough for a clear picture to emerge, and it is in this light that we opt to lean to the side of consistency among large but independent data sets, like those from the satellite limb collection, as validation source. The definition of a limb-based reference for stratospheric NO₂ allows us to make inferences about the quality of other data sets. For instance, the simulated stratospheric NO₂ columns from WACCM match the limb reference neatly over the tropics. However, simulated columns are high in the extratropics, particularly in the Northern Hemisphere, with positive biases of 1.0×10^{15} molecules cm⁻², or 35 % relative to the limb reference. The stratospheric NO₂ columns from the SCIAMACHY nadir record are negatively biased by -0.5×10^{15} molecules cm⁻², or -20 % relative to the limb reference. The stratospheric NO₂ columns from OMI are positively biased by 0.6×10^{15} molecules cm⁻², or +20 % relative to the limb reference.

The last part of this work examines how biases in slant columns retrieved from nadir instruments are assimilated largely into the stratospheric component, and not expected to affect tropospheric columns significantly, as long as they are additive errors. It also considers the seasonal variability of the stratospheric air mass factor and its sensitivity to errors in the a priori gas and temperature profiles, to justify that errors in stratospheric columns may safely be attributed to errors in the total slant column – related to algorithm and/or instrumental effects. A brief look at the longitudinal distribution of nadir-to-limb discrepancies also suggests the presence of temperature-correlated errors in the nadir stratospheric NO₂ retrievals from OMI and SCIAMACHY.

There is a general lack of consensus regarding absolute slant columns derived from nadir instruments using different retrieval methodologies. It becomes clear that stratospheric NO₂ columns derived from nadir instruments like SCIAMACHY and OMI are affected by seasonally and latitudinally dependent biases that are sensitive to the retrieval configuration used to generate them (i.e., wavelength calibration,

absorption cross sections for NO₂, spectral fit window width, number of interfering species, spectral resolution, solar reference spectra, ring spectra, etc.). The remarkable diversity in DOAS approaches currently available to carry out slant retrievals from nadir instruments (e.g., from IUP Bremen: Hillboll et al., 2013; from MPI-Heidelberg: Beirle et al., 2010; from KNMI: Boersma et al., 2007; from BIRA-IASB) points to the necessity to perform a critical review of retrieval methodologies, if anything to clarify whether biases are algorithm or instrument/calibration related. These biases render stratospheric NO₂ products from nadir instruments suboptimal for scientific studies, and call for urgent attention, given that limb techniques are giving way to nadir techniques as the next generation of climate and air quality monitoring instruments. Such an effort towards harmonization, which is already underway as part of the pre-launch characterization for the Tropospheric Monitoring Instrument (TROPOMI), is required to promote the utilization of nadir stratospheric NO₂ columns for ozone studies and climate research.

Acknowledgements. The authors gratefully acknowledge the assistance of A. Rozanov, G. Stiller and D. Kinnison in providing access to and facilitating the interpretation of the SCIAMACHY limb, MIPAS and WACCM records. This work has been funded by the Netherlands Space Office (NSO) under OMI contract.

Edited by: M. Van Roozendael

References

- Bauer, R., Rozanov, A., McLinden, C. A., Gordley, L. L., Lotz, W., Russell III, J. M., Walker, K. A., Zawodny, J. M., Ladstätter-Weißmayer, A., Bovensmann, H., and Burrows, J. P.: Validation of SCIAMACHY limb NO₂ profiles using solar occultation measurements, *Atmos. Meas. Tech.*, 5, 1059–1084, doi:10.5194/amt-5-1059-2012, 2012.
- Beirle, S., Kühl, S., Pukite, J., and Wagner, T.: Retrieval of tropospheric column densities of NO₂ from combined SCIAMACHY nadir/limb measurements, *Atmos. Meas. Tech.*, 3, 283–299, doi:10.5194/amt-3-283-2010, 2010.
- Boersma, K. F., Eskes, H. J., and Brinksma, E. J.: Error analysis for tropospheric NO₂ retrieval from space, *J. Geophys. Res.*, 109, D04311, doi:10.1029/2003JD003962, 2004.
- Boersma, K. F., Eskes, H. J., Veefkind, J. P., Brinksma, E. J., van der A, R. J., Sneep, M., van den Oord, G. H. J., Levelt, P. F., Stammes, P., Gleason, J. F., and Bucsela, E. J.: Near-real time retrieval of tropospheric NO₂ from OMI, *Atmos. Chem. Phys.*, 7, 2103–2118, doi:10.5194/acp-7-2103-2007, 2007.
- Boersma, K. F., Jacob, D. J., Eskes, H. J., Pinder, R. W., Wang, J., and van der A, R.: Intercomparison of SCIAMACHY and OMI tropospheric NO₂ columns: Observing the diurnal evolution of chemistry and emissions from space, *J. Geophys. Res.*, 113, 1–14, 2008.
- Boersma, K. F., Eskes, H. J., Dirksen, R. J., van der A, R. J., Veefkind, J. P., Stammes, P., Huijnen, V., Kleipool, Q. L., Sneep, M., Claas, J., Leitão, J., Richter, A., Zhou, Y., and Brun-

- ner, D.: An improved tropospheric NO₂ column retrieval algorithm for the Ozone Monitoring Instrument, *Atmos. Meas. Tech.*, 4, 1905–1928, doi:10.5194/amt-4-1905-2011, 2011.
- Bogumil, K., Orphal, J., Homann, T., Voigt, S., Spietz, P., Fleischmann, O. C., Vogel, A., Hartmann, M., Kromminga, H., Bovensmann, H., Frerick, J., and Burrows, J. P.: Measurements of molecular absorption spectra with the SCIAMACHY Pre-Flight Model: instrument characterization and reference data for atmospheric remote sensing in the region 230–2380 nm region, *J. Photochem. Photobiol. A Chem.*, 157, 167–184, 2003.
- Bovensmann, H., Burrows, J. P., Buchwitz, M., Frerick, J., Noël, S., Rozanov, V. V., Chance, K. V., Goede, A. P. H.: SCIAMACHY: mission objectives and measurement modes, *J. Atmos. Sci.*, 56, 127–150, 1999.
- Bracher, A., Bovensmann, H., Bramstedt, K., Burrows, J. P., von Clarmann, T., Eichmann, K. U., Fischer, H., and Funke, B.: Cross-comparisons of O₃ and NO₂ measured by the atmospheric ENVISAT instruments GOMOS, MIPAS and SCIAMACHY, *Adv. Space Res.*, 36, 855–867, 2005.
- Brasseur, G. P. and Solomon, S.: *Aeronomy of the Middle Atmosphere: Chemistry and Physics of the Stratosphere and Mesosphere*, Springer, 2005.
- Brasseur, G. P., Orlando, J. J., and Tyndall, G. S.: *Atmospheric Chemistry and Global Change*, Oxford University Press, 1999.
- Bucsela, E. J., Krotkov, N. A., Celarier, E. A., Lamsal, L. N., Swartz, W. H., Bhartia, P. K., Boersma, K. F., Veefkind, J. P., Gleason, J. F., and Pickering, K. E.: A new stratospheric and tropospheric NO₂ retrieval algorithm for nadir-viewing satellite instruments: applications to OMI, *Atmos. Meas. Tech.*, 6, 2607–2626, doi:10.5194/amt-6-2607-2013, 2013.
- Burrows, J. P., Platt, U., and Borrell, P. (Eds.): *The Remote Sensing of Tropospheric Composition From Space*, Springer, 2011.
- Chance, K. (Ed.): *OMI Algorithm Theoretical Basis Document: OMI Trace Gas Algorithms, ATBD-OMI-02, Version 2.0, Volume 4*, available at: www.temis.nl/airpollution/no2.html (last access: January 2014), 2002.
- Cook, P. A. and Roscoe, H. K.: Variability and trends in stratospheric NO₂ in Antarctic summer and implications for stratospheric NO_y, *Atmos. Chem. Phys.*, 9, 3601–3612, doi:10.5194/acp-9-3601-2009, 2009.
- Dirksen, R., Dobber, M. R., Voors, R., and Levelt, P.: Pre-launch characterization of the Ozone Monitoring Instrument transfer function in the spectral domain, *Appl. Optics*, 45, 3972–3981, 2006.
- Dirksen, R. J., Boersma, K. F., Eskes, H., Ionov, D. V., Bucsela, E. J., Levelt, P. F., and Kelder, H. M.: Evaluation of stratospheric NO₂ retrieved from the Ozone Monitoring Instrument: intercomparison, diurnal cycle and trending, *J. Geophys. Res.*, 116, D08305, doi:10.1029/2010JD014943, 2011.
- Eskes, H. J. and Boersma, K. F.: Averaging kernels for DOAS total-column satellite retrievals, *Atmos. Chem. Phys.*, 3, 1285–1291, doi:10.5194/acp-3-1285-2003, 2003.
- Eyring, V., Shepherd, T. G., and Waugh, D. W. (Eds.): *SPARC Report on the Evaluation of Chemistry-Climate Models*, SPARC Report No. 5, WCRP-132, WMO/TD-No. 1526, 2010.
- Farman, J. C., Gardiner, B. G., and Shanklin, J. D.: Large losses of total ozone in Antarctica reveal seasonal ClO_x/NO_x interaction, *Nature*, 315, 207–210, 1985.
- Fischer, H., Birk, M., Blom, C., Carli, B., Carlotti, M., von Clarmann, T., Delbouille, L., Dudhia, A., Ehrt, D., Endemann, M., Flaud, J. M., Gessner, R., Kleinert, A., Koopman, R., Langen, J., López-Puertas, M., Mosner, P., Nett, H., Oelhaf, H., Perron, G., Remedios, J., Ridolfi, M., Stiller, G., and Zander, R.: MIPAS: an instrument for atmospheric and climate research, *Atmos. Chem. Phys.*, 8, 2151–2188, doi:10.5194/acp-8-2151-2008, 2008.
- Funke, B., Lopez-Puertas, M., von Clarmann, T., Stiller, G. P., Fischer, H., Glatthor, N., Grabowski, U., Hopfner, M., Kellman, S., Kiefer, M., Linden, A., Mengistu Tsidu, G., Milz, M., Steck, T., and Wang, D. Y.: Retrieval of stratospheric NO_x from 5.3 and 6.2 micrometer nonlocal thermodynamic equilibrium emissions measured by Michelson Interferometer for Passive Atmospheric Sounding (MIPAS) on Envisat, *J. Geophys. Res.*, 110, D09302, doi:10.1029/2004JD005225, 2005.
- Garcia, R. R., Marsh, D. R., Kinnison, D. E., Boville, B. A., and Sassi, F.: Simulations of secular trends in the middle atmosphere, *J. Geophys. Res.*, 112, D09301, doi:10.1029/2006JD007485, 2007.
- Gille, J. C., Barnett, J., Whitney, J., Dials, M., Woodard, D., Rudolf, W., Lambert, A., and Mankin, W.: The High Resolution Dynamics Limb Sounder (HIRDLS) Experiment on Aura, *P. SPIE IS&T Elect. Im.*, 5152, 162–171, 2003.
- Gille, J. C., Barnett, J., Arter, P., Barker, M., Bernath, P., Boone, C., Cavanaugh, C., Chow, J., Coffey, M., Craft, J., Craig, C., Dials, M., Dean, V., Eden, T., Edwards, D. P., Francis, G., Halvorson, C., Harvey, L., Hepplewhite, C., Khosravi, R., Kinnison, D., Krinsky, C., Lambert, A., Lee, H., Lyjak, L., Loh, J., Mankin, W., Massie, S., McInerney, J., Moorhouse, J., Nardi, B., Packman, D., Randall, C., Reburn, J., Rudolf, W., Schwartz, M., Serafin, J., Stone, K., Torpy, B., Walker, K., Waterfall, A., Watkins, R., Whitney, J., Woodard, D., and Young, G.: The High Resolution Dynamics Limb Sounder: experiment overview, recovery and validation of initial temperature data, *J. Geophys. Res.*, 113, D16S43, doi:10.1029/2007JD008824, 2008.
- Gille, J. C., Gray, L., Cavanaugh, C., Dean, V., Karol, S., Kinnison, D., Nardi, B., Smith, L., Waterfall, A., Coffey, M., Halvorson, C., Khosravi, R., Massie, S., Belmonte Rivas, M., Torpy, B., and Wright, C.: *HIRDLS EOS Data Description and Quality Document – Version 7*, available at: <http://disc.sci.gsfc.nasa.gov/Aura/data-holdings/HIRDLS/documents/HIRDLS-V7-DQD.pdf> (last access: January 2014), 2012a.
- Gille, J. C., Cavanaugh, C., Halvorson, C., Hartsough, C., Nardi, B., Belmonte Rivas, M., Khosravi, R., Smith, L., and Francis, G.: Final correction algorithms for HIRDLS version 7 data, *P. SPIE IS&T Elect. Im.*, 8511, 85110K, doi:10.1117/12.930175, 2012b.
- Hegglin, M. I. and Tegtmeier, S. (Eds.): *SPARC Data Initiative Report on the Evaluation of Trace Gas and Aerosol Climatologies From Satellite Limb Sounders*, in preparation, 2014.
- Hendrick, F., Mahieu, E., Bodeker, G. E., Boersma, K. F., Chipperfield, M. P., De Mazière, M., De Smedt, I., Demoulin, P., Fayt, C., Hermans, C., Kreher, K., Lejeune, B., Pinardi, G., Servais, C., Stübi, R., van der A, R., Vernier, J.-P., and Van Roozendael, M.: Analysis of stratospheric NO₂ trends above Jungfraujoch using ground-based UV-visible, FTIR, and satellite nadir observations, *Atmos. Chem. Phys.*, 12, 8851–8864, doi:10.5194/acp-12-8851-2012, 2012.
- Hilboll, A., Richter, A., Rozanov, A., Hodnebrog, Ø., Heckel, A., Solberg, S., Stordal, F., and Burrows, J. P.: Improvements to the

- retrieval of tropospheric NO₂ from satellite – stratospheric correction using SCIAMACHY limb/nadir matching and comparison to Oslo CTM2 simulations, *Atmos. Meas. Tech.*, 6, 565–584, doi:10.5194/amt-6-565-2013, 2013.
- Houweling, S., Dentener, F. J., and Lelieveld, J.: The impact of non-methane hydrocarbon compounds on tropospheric chemistry, *J. Geophys. Res.*, 103, 10673–10696, 1998.
- Kinnison, D. E., Brasseur, G. P., Walters, S., Garcia, R. R., Marsh, D., Sassi, F., Harvey, L., Randall, C., Emmons, L., Lamarque, J. F., Hess, P., Orlando, J., Tie, X. X., Randell, W., Pan, L. L., Gettelman, A., Granier, C., Diehl, T., Niemeier, O., and Simmons, A. J.: Sensitivity of chemical tracers to meteorological parameters in the MOZART-3 chemical transport model, *J. Geophys. Res.*, 112, D20302, doi:10.1029/2006JD007879, 2007.
- Knudsen, B. M.: On the accuracy of analysed low temperatures in the stratosphere, *Atmos. Chem. Phys.*, 3, 1759–1768, doi:10.5194/acp-3-1759-2003, 2003.
- Krotkov, N. A., Bucsela, E. J., Celarier, E. A., Lamsal, L. N., and Swartz, W. H.: Improved OMI NO₂ Standard Product: Algorithm, evaluation, and results, EOS Aura Science Team Meeting, Pasadena, California, 1–3 October, 2012.
- Krotkov, N. A., Joiner, J., Bhartia, P. K., Lamsal, L. N., Marchenko, S., Celarier, E. A., Swartz, W. H., and Li, C.: Key improvements in OMI NO₂ and SO₂ products, 18th OMI Science Team Meeting, De Bilt, Netherlands, 11–13 March, 2014.
- Lamarque, J. F., Brasseur, G. P., Hess, P. G., and Muller, J. F.: Three-dimensional study of the relative contributions of the different nitrogen sources in the troposphere, *J. Geophys. Res.*, 101, 22955–22968, 1996.
- Lambert, A., Bailey, P. L., Edwards, D. P., Gille, J. C., Johnson, B. R., Halvorson, C. M., Massie, S. T., and Stone, K. A.: High Resolution Dynamics Limb Sounder, Level-2 Algorithm Theoretical Basis Document, available at: <http://eosps.gsfc.nasa.gov/sites/default/files/atbd/ATBD-HIR-02.pdf> (last access: January 2014), 1999.
- Levelt, P. J., Gijsbertus, H., van den Oord, J., Dobber, M. R., Malkki, A., Visser, H., de Vries, J., Stammes, P., Lundell, J. O. V., and Saari, H.: The Ozone Monitoring Instrument, *IEEE T. Geosci. Remote*, 44, 1093–1101, 2006.
- Louis, J. F.: A parametric model of vertical eddy fluxes in the atmosphere, *Bound.-Lay. Meteorol.*, 17, 187–202, 1979.
- McLinden, C. A., Haley, C. S., and Sioris, C. E.: Diurnal effects in limb scatter observations, *J. Geophys. Res.*, 111, D14302, doi:10.1029/2005JD006628, 2000.
- Noxon, J. F.: Stratospheric NO₂: global behavior, *J. Geophys. Res.*, 84, 5067–5076, doi:10.1029/JC084iC08p05067, 1979.
- Olivier, J., Peters, J., Granier, C., Petron, G., Müller, J. F., and Walens, S.: Present and Future Emissions of Atmospheric Compounds, POET report #2, EU report EV K2-1999-00011, 2003.
- Palmer, P. I., Jacob, D. J., Chance, K., Martin, R. V., Spurr, R. J. D., Kurosu, T. P., Bey, L., Yantosca, R., Fiore, A., and Li, Q.: Air mass factor formulation for spectroscopic measurements from satellites: application to formaldehyde retrievals from the Global Ozone Monitoring Experiment, *J. Geophys. Res.*, 106, 14539–14550, 2001.
- Ravishankara, A. R., Daniel, J. S., and Portmann, R. W.: Nitrous oxide (N₂O): the dominant ozone depleting substance emitted in the 21st century, *Science*, 326, 123–125, 2009.
- Richter, J. H., Sassi, F., Garcia, R. R., Matthes, K., and Fischer, C. A.: Dynamics of the middle atmosphere as simulated by the Whole Atmosphere Community Climate Model, version 3 (WACCM3), *J. Geophys. Res.*, 113, D08101, doi:10.1029/2007JD009269, 2008.
- Rienecker, M. M., Suarez, M. J., Gelaro, R., Todling, R., Bacmeister, J., Liu, E., Bosilovich, M. G., Schubert, S. D., Takacs, L., Kim, G. K., Bloom, S., Chen, J., Collins, D., Conaty, A., da Silva, A., Gu, W., Joiner, J., Koster, R., Lucchesi, R., Molod, A., Owens, T., Pawson, S., Pegion, P., Redder, C., Reichle, R., Robertson, F., Ruddick, A. G., Sienkiewicz, M., and Woolen, J.: MERRA: NASA's Modern-Era Retrospective Analysis for Research and Applications, *J. Climate*, 24, 3624–3648, 2011.
- Rosenlof, K. H.: Seasonal cycle of the residual mean meridional circulation in the stratosphere, *J. Geophys. Res.*, 100, 5173–5191, 1995.
- Rozanov, A.: Product Specification Document: NO₂ Version 3.1, available at: http://www.iup.uni-bremen.de/~sciapro/CDI/DOCU/Algorithm_Document.pdf (last access: January 2014), 2008.
- Russel, G. and Lerner, J.: A new finite-differencing scheme for the tracer transport equation, *J. Appl. Meteorol.*, 20, 1483–1498, 1981.
- Solomon, S. and Garcia, R. R.: On the distribution of nitrogen dioxide in the high-latitude stratosphere, *J. Geophys. Res.*, 88, 5229–5239, 1983.
- Solomon, S., Mount, G. H., and Zawodny, J. M.: Measurements of stratospheric NO₂ from the Solar Mesosphere Explorer Satellite, 2. General morphology of observed NO₂ and derived N₂O₅, *J. Geophys. Res.*, 89, 7317–7321, 1984.
- Tiedtke, M.: A comprehensive mass flux scheme for cumulus parameterization in large-scale models, *Mon. Weather Rev.*, 117, 1779–1800, 1989.
- Vandaele, A. C., Hermans, C., Simon, P. C., Carleer, M., Colin, R., Fally, S., Merienne, M. F., Jenouvrier, A., and Coquart, B.: Measurements of the NO₂ absorption cross-section from 42 000 cm⁻¹ to 10 000 cm⁻¹ (238–1000 nm) at 220 K and 294 K, *J. Quant. Spectrosc. Ra.*, 59, 171–184, 1998.
- van der A, R. J., Eskes, H. J., van Roozendael, M., De Smedt, I., Blond, N., Boersma, F. K., Weiss, A., and van Peet, J. C. A.: Algorithm document: tropospheric NO₂, TEM/AD1/001, Royal Netherlands Meteorology Institute, De Bilt, the Netherlands, available at: www.temis.nl/airpollution/no2.html (last access: January 2014), 2006.
- von Clarmann, T., Chidzie Chineke, T., Fischer, H., Funke, B., Garcia-Comas, M., Gil-Lopez, S., Glatthor, N., Grabowski, U., Hopfner, M., Kellmann, S., Kiefer, M., Linden, A., Lopez-Puertas, M., Lopez-Valverde, M. A., Mengistu Tsidu, G., Milz, M., Steck, T., and Stiller, G. A.: Remote sensing of the middle atmosphere with MIPAS, *P. SPIE IS&T Elect. Im.*, 4882, 172–183, 2003.
- Vountas, M., Rozanov, V. V., Richter, A., and Burrows, J. P.: Ring Effect: Impact of rotational Raman Scattering on Radiative Transfer in Earth's Atmosphere, *J. Quant. Spec. Rad. Transf.*, 60, 943–961, 1998.
- Wennberg, P. O., Cohen, R. C., Stimpfle, R. M., Koplow, J. P., Anderson, J. G., Salawitch, R. J., Fahey, D. W., Woodbridge, E. L., Keim, E. R., Gao, R. S., Webster, C. R., May, R. D., Toohey, D., Avallone, L., Proffitt, M. H., Loewenstein, M., Podolske, J. R.,

- Chan, K. R., and Wofsy, S. C.: Removal of stratospheric O₃ by radicals: in situ measurements of OH, HO₂, NO, NO₂, ClO and BrO, *Science*, 266, 398–404, 1994.
- Wetzel, G., Bracher, A., Funke, B., Goutail, F., Hendrick, F., Lambert, J.-C., Mikuteit, S., Piccolo, C., Pirre, M., Bazureau, A., Belotti, C., Blumenstock, T., De Mazière, M., Fischer, H., Huret, N., Ionov, D., López-Puertas, M., Maucher, G., Oelhaf, H., Pommereau, J.-P., Ruhnke, R., Sinnhuber, M., Stiller, G., Van Roozendaal, M., and Zhang, G.: Validation of MIPAS-ENVISAT NO₂ operational data, *Atmos. Chem. Phys.*, 7, 3261–3284, doi:10.5194/acp-7-3261-2007, 2007.
- World Meteorological Organization: Scientific Assessment of Ozone Depletion, Geneva, Switzerland, 2003.
- Zawodny, J. M. and McCormick, M. P.: Stratospheric Aerosol and Gas Experiment II measurements of the quasi-biennial oscillations in ozone and nitrogen dioxide, *J. Geophys. Res.*, 96, 9371–9377, doi:10.1029/91JD00517, 1991.